Supplementary Information

for

$AgBiS_2$ Nanocrystal Synthesis from Molecular Precursors: Insights into the Acid-Catalyzed Decomposition of Dialkyldithiocarbamate Ligands

Annie Regan,[1] Vaishali Kshirsagar,[1] Paul F. Gramelspacher,[1] Thomas J. Boggess,[1] Anuraj Kshirsagar,[1] Charles Edwin Webster[1]*, and Sidney E. Creutz[1]*

1. Department of Chemistry, Mississippi State University, Mississippi State, MS 39762, USA.

*Corresponding authors, email: ewebster@chemistry.msstate.edu, screutz@chemistry.msstate.edu

Table of Contents

I. Additional PXRD data for $AgBiS_2$ synthesized under different conditions

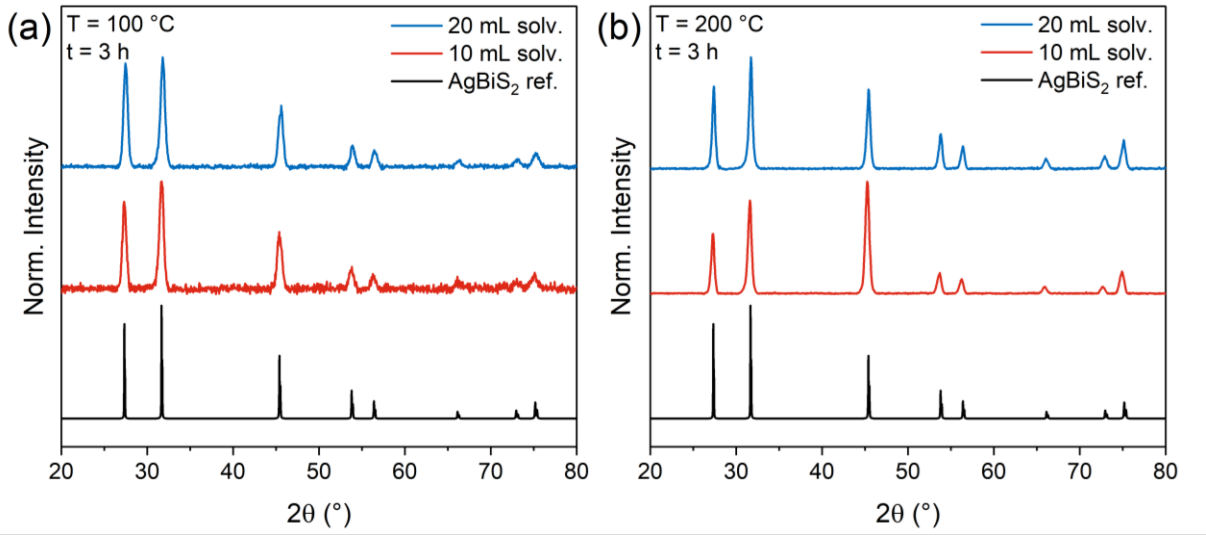

Figure S1: Powder XRD patterns of $AgBiS_2$ produced by thermal decomposition of diethyldithiocarbamate metal precursors in a 1:1 mixture of octadecene (ODE) and oleylamine (OLA) at both (a) 100 °C and (b) 200 °C to investigate the effect of solvent/ligand concentration. Reference pattern obtained from COD (#9011025).

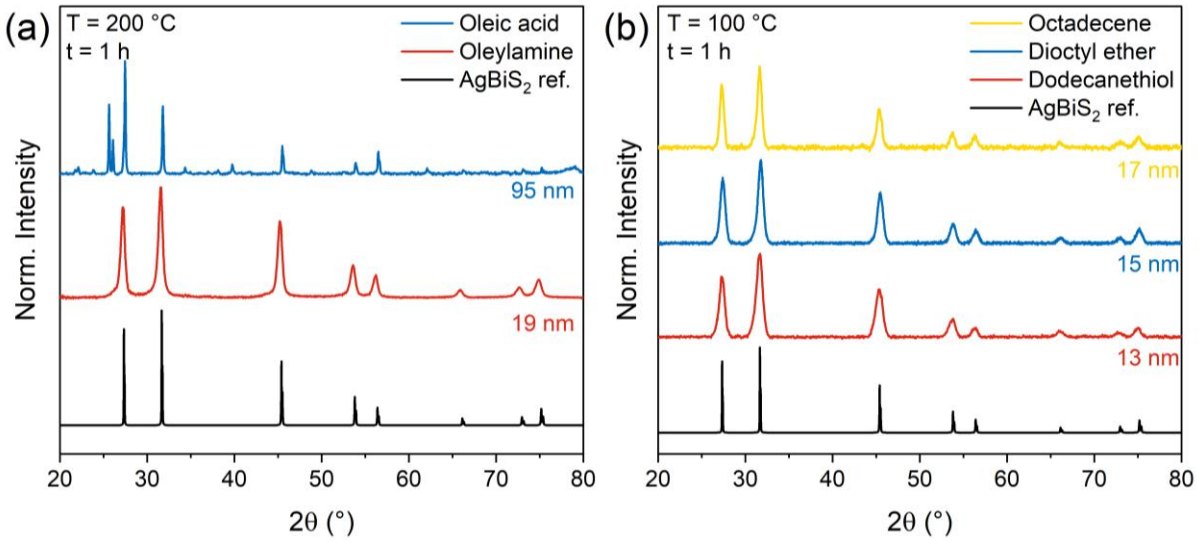

Figure S2: Powder XRD patterns of $AgBiS_2$ produced by thermal decomposition of diethyldithiocarbamate metal precursors in a 1:1 mixture of (a) octadecene (ODE) and either oleylamine (OLA) or oleic acid (OA), to investigate the effect of ligand type, and (b) oleylamine (OLA) and either octadecene (ODE), dioctyl ether (DE), or dodecanethiol (DDT), to investigate the effect of solvent type. Reference pattern obtained from COD (#9011025).

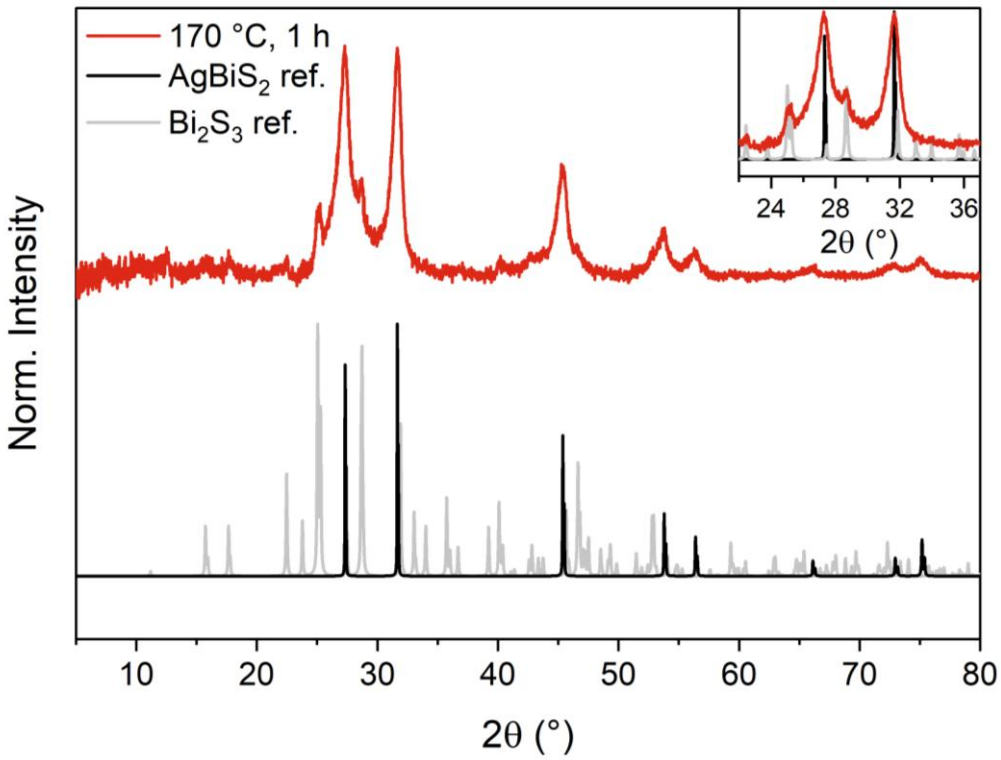

Figure S3: Powder XRD pattern of $AgBiS_2$ produced by thermal decomposition of diisopropyldithiocarbamate metal precursors in a 1:1 mixture of octadecene (ODE) and oleylamine (OLA) to investigate the effect of DTC-ligand type on the metal precursors. Inset highlights impurity peaks matched to Bi_2S_3 with adjusted intensities for clarity. Reference patterns obtained from COD and ICSD ($AgBiS_2$ #9011025, Bi_2S_3 #153946).

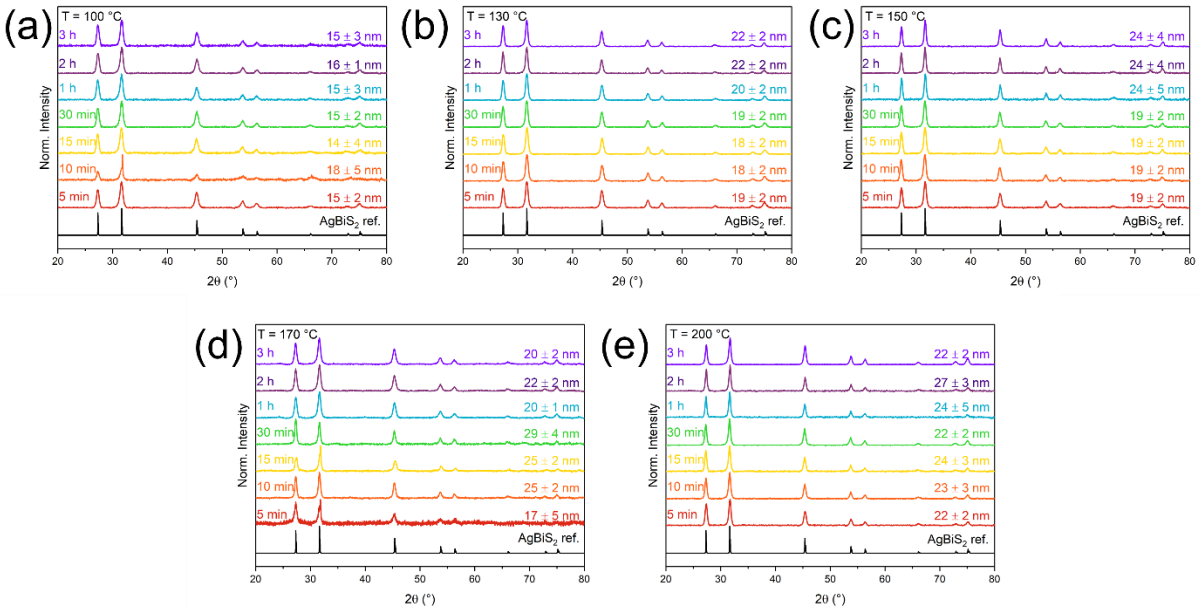

Figure S4: Powder XRD patterns of $AgBiS_2$ produced by thermal decomposition in a solvent/ligand mixture of 1:1 OLA/ODE at (a) 100 °C, (b) 130 °C, (c) 150 °C, (d) 170 °C, and (e) 200 °C, showing average crystallite size and corresponding standard deviation for each. Each reaction was performed over 3 h, with 0.3 mL aliquots being extracted over a time series of 5 mins to 180 mins after the internal reaction temperature reaching the desired set-point. Reference pattern obtained from COD (#9011025).

Table S1. Scherrer crystallite sizes of $AgBiS_2$ measured for each sample's diffraction pattern shown in Fig. S4, presented as a function of temperature and time.

Temperature (°C)	5 min	10 min	15 min	30 min	60 min	120 min	180 min
100	15 nm	18 nm	14 nm	15 nm	15 nm	16 nm	15 nm
130	19 nm	18 nm	18 nm	19 nm	20 nm	22 nm	22 nm
150	19 nm	19 nm	19 nm	19 nm	24 nm	24 nm	24 nm
170	17 nm	25 nm	25 nm	29 nm	20 nm	22 nm	20 nm
200	22 nm	23 nm	24 nm	22 nm	24 nm	27 nm	22 nm

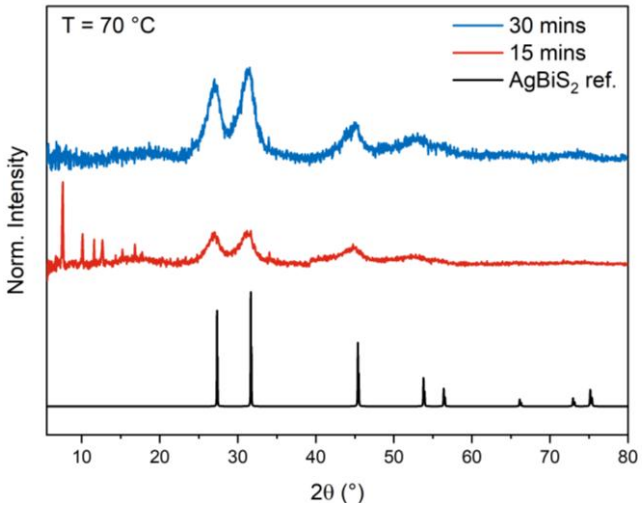

Figure S5: Powder XRD patterns of $AgBiS_2$ produced by thermal decomposition in a solvent/ligand mixture of OLA/DDT (1:1 mole ratio) at 70 °C for 15 mins vs. 30 mins. Reaction was performed at standard scale.

II. Analysis of lamellar phase periodicity

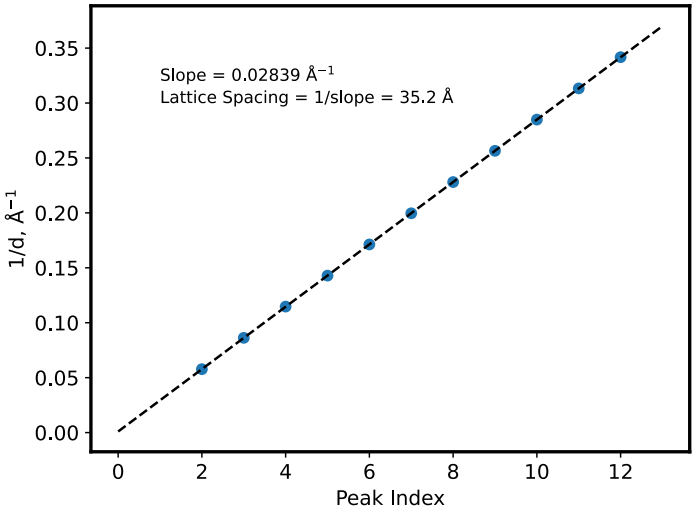

Figure S6. Periodicity of the lamellar phase, as observed in the "0 minute" sample from the $AgBiS_2$ synthesis in OLA/DDT (1:1 mole ratio) at 70 °C (as shown in Figure 6 in the main text). The peak positions of the sharp repeating features (using the $K_{\alpha 1}$ lines) were converted to *d*-spacing and plotted against the peak index, shifted to pass through the origin.[1] The spacing of the lamellar sheets is determined to be 35.2 Å.

III. Rietveld analysis of $AgBiS_2$ PXRD data

Rietveld Refinement: Rietveld refinement was carried out with the program Profex version 5.5.1 using the refinement kernel BGMN.[2] The program calculates the instrument peak profiles using the Fundamental Parameters Approach based on the instrument configuration. Unless otherwise stated below for particular cases, peak broadening was modeled as resulting only from particle size effects (i.e., strain effects were neglected), and the particle sizes were refined anisotropically. Texture effects were modeled using sixth-order spherical harmonics. Lattice parameters for the structures were allowed to refine within ±1% of the reported values. Thermal displacement parameters for the atoms were refined anisotropically; atomic positions and occupancies were not refined and were fixed at reported values. For minor phases (Ag_2S in several of the samples), particle size and thermal displacement parameters were refined isotropically and texture effects were neglected. A sample displacement error factor was also included in the refinements. The background was modeled as a combination of a scaled measured background from an empty sample plate and a polynomial background function.

Figure S7 shows Rietveld refinement of a representative sample from the synthesis in OLA/ODE, carried out at 200 °C with a 5-minute reaction time. The data was modeled with the cubic schapbachite $AgBiS_2$ structure (COD entry 9011025) and no evidence for additional phases was found. Attempting to include alternative phases including Ag_2S (argentite or acanthite), Bi_2S_3 (bismuthinite), $AgBi_3S_5$ (pavonite), or other phases of $AgBiS_2$ (matildite) did not significantly improve the fit and/or refined to 0% content of the minor phase. Some unmodeled intensity near 29° may be due to amorphous scattering (e.g., from organic ligands), which typically results in some scattered intensity in this region.

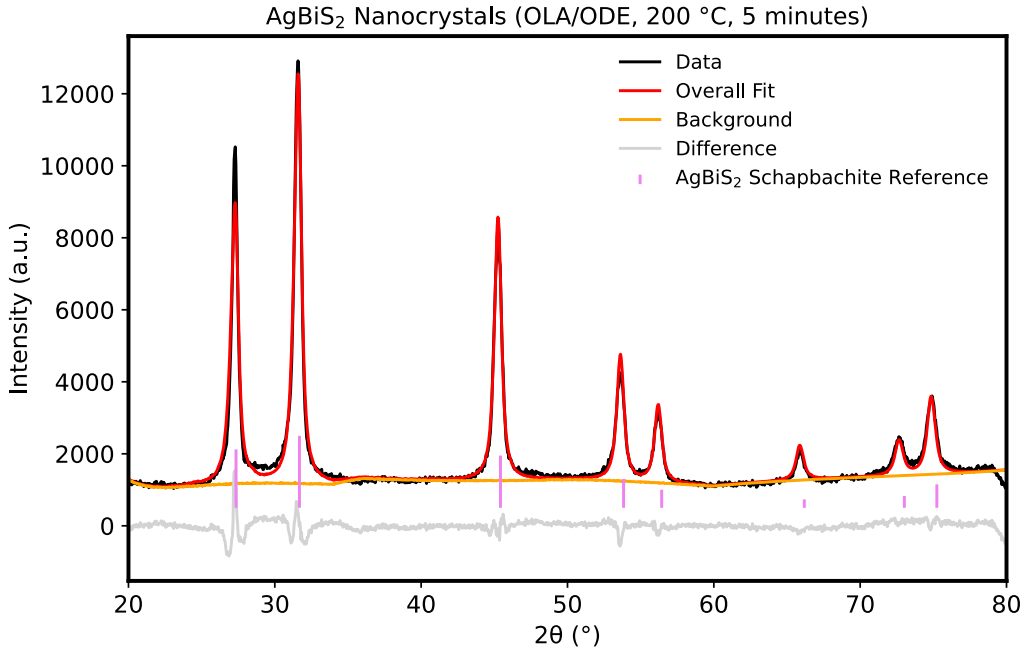

Figure S7. Powder XRD data and refinement for a sample of $AgBiS_2$ nanocrystals prepared using the standard method in OLA/ODE at 200 °C with a 5-minute reaction time. The crystalline grain size determined by refinement of this sample is 19 ± 0.3 nm.

Figures S8 and S9 show Rietveld refinements of two samples of $AgBiS_2$ nanocrystals synthesized at 70 °C in an equimolar mixture of OLA:DDT. These were modeled as a mixture of $AgBiS_2$ (schapbachite) and Ag_2S (acanthite). Attempting to include other phases such as matildite, argentite, or bismuthinite did not improve the fit.

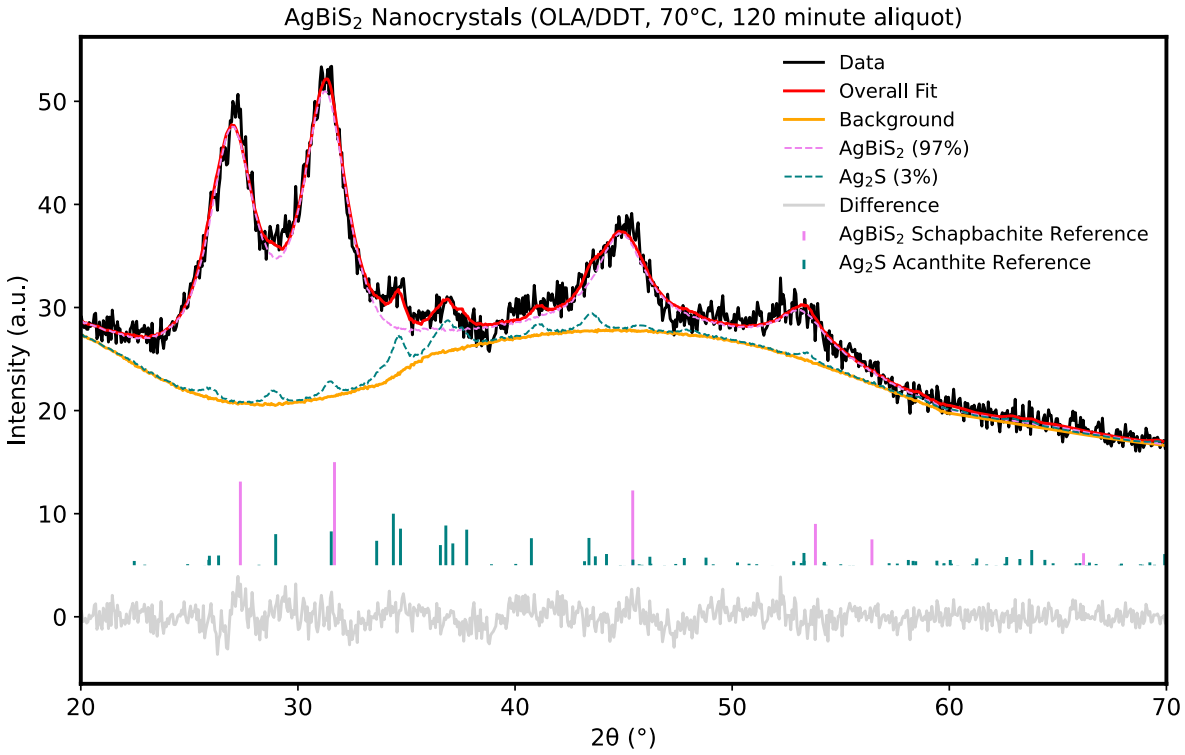

Figure S8. Powder XRD data and refinement for a sample of $AgBiS_2$ nanocrystals prepared at 70 °C in OLA/DDT; this sample was part of the aliquot study shown in Figure 6 of the main text and was taken after 120 minutes of reaction time. The sample was refined to include a 3% Ag_2S impurity. The $AgBiS_2$ crystalline grain size determined by refinement of this sample is 3.0 ± 0.05 nm.

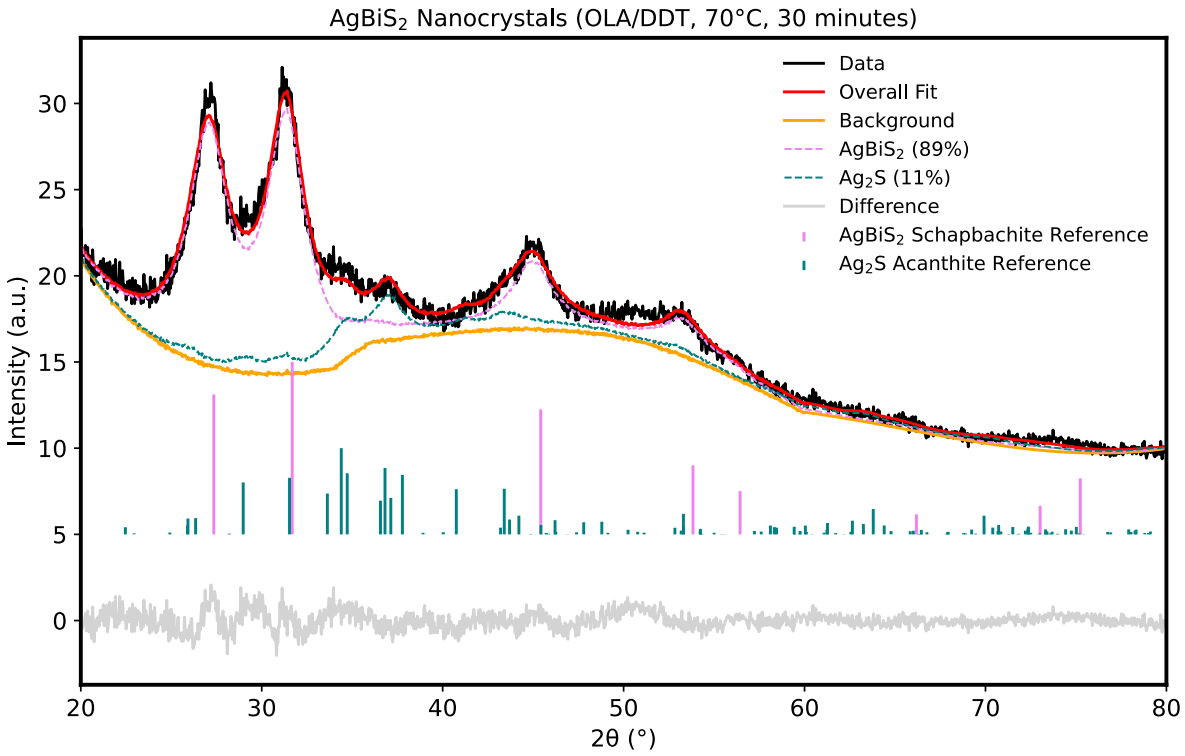

Figure S9. Powder XRD data and refinement for a sample of $AgBiS_2$ nanocrystals prepared using the standard method in OLA/DDT at 70 °C with a 30-minute reaction time. The sample was refined to include an 11% Ag_2S impurity. The $AgBiS_2$ crystalline grain size determined by refinement of this sample is 3.0 ± 0.1 nm.

Figure S10 shows Rietveld refinements of $AgBiS_2$ nanocrystals synthesized at 70 °C in OLA in the presence of two equivalents of added diethylammonium N,N-diethyldithiocarbamate. Attempting to include an Ag_2S (acanthite) component in the fit did slightly improve the refinement (Figure S10A), but with a high uncertainty for the Ag_2S content; since there are no well-defined peaks, it is difficult to assign the modeled intensity to Ag_2S *vs*. other potential amorphous or poorly crystalline species or background features.

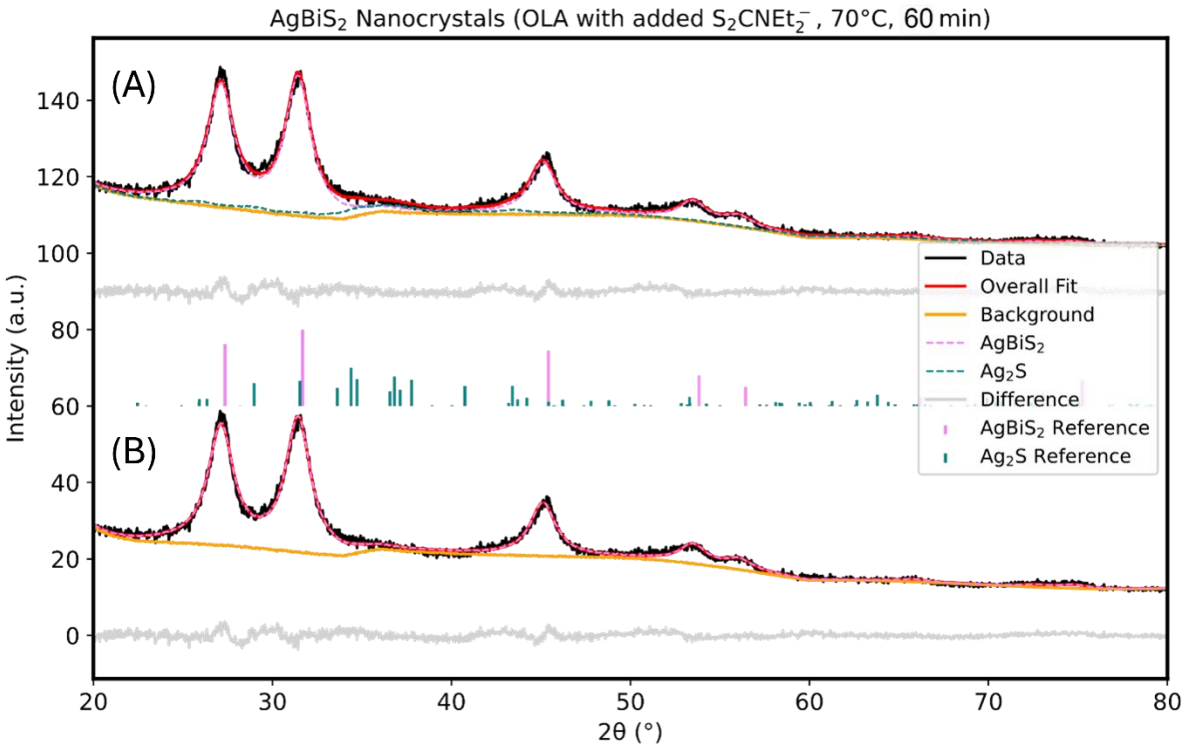

Figure S10. PXRD Rietveld refinements of $AgBiS_2$ nanocrystals synthesized at 70 °C in OLA in the presence of added diethylammonium N,N-diethyldithiocarbamate. Refinement was carried out both (a) with and (b) without allowing for an Ag_2S impurity. The crystalline grain size of $AgBiS_2$ determined from the fitting is 4.8 ± 0.3 nm.

Figure S11 shows Rietveld refinements of $AgBiS_2$ nanocrystals synthesized at 70 °C in OLA in the presence of two equivalents of CS_2. It was modeled as a mixture of $AgBiS_2$ (schapbachite) and Ag_2S (acanthite). Attempting to include other phases such as matildite, argentite, or bismuthinite did not improve the fit.

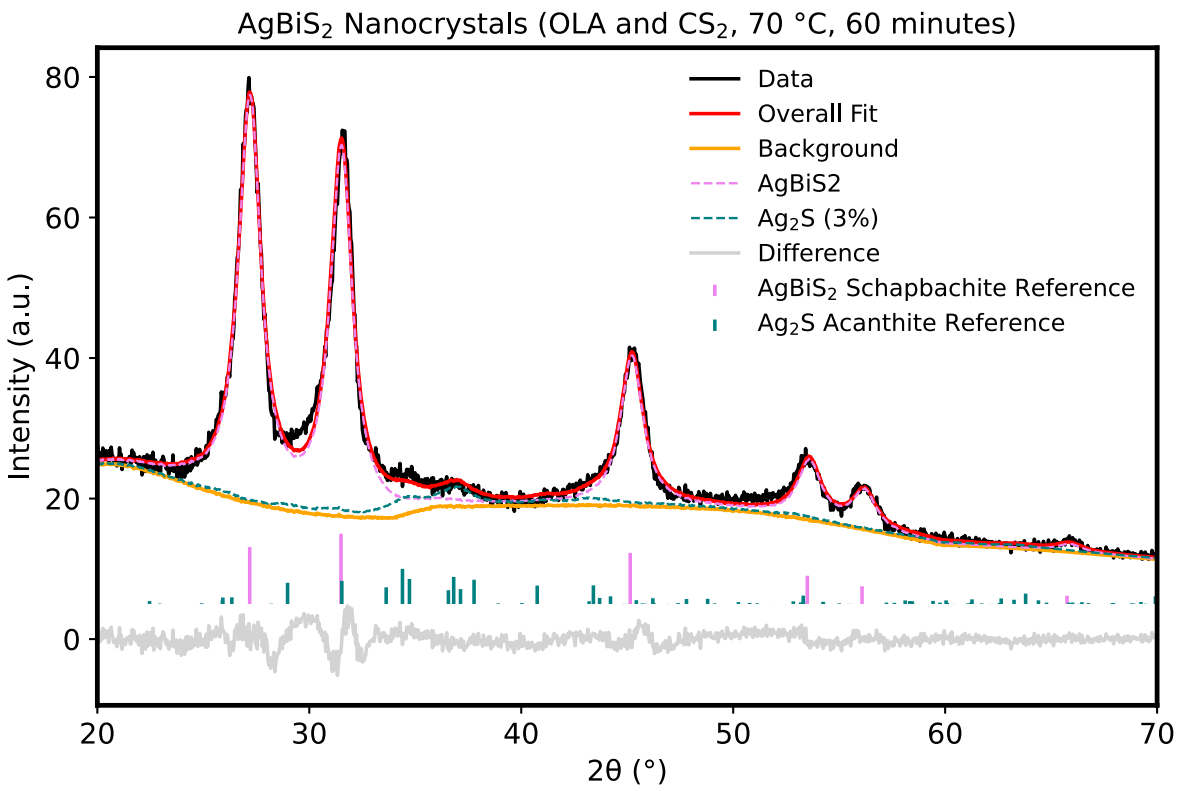

Figure S12. PXRD Rietveld refinements of $AgBiS_2$ nanocrystals synthesized at 70 °C in OLA in the presence of added carbon disulfide. The sample was refined to include an 8% Ag_2S impurity. The $AgBiS_2$ crystalline grain size determined by refinement of this sample is 6.8 ± 0.1 nm.

IV. TEM/EDX mapping data for AgBiS2 nanocrystals

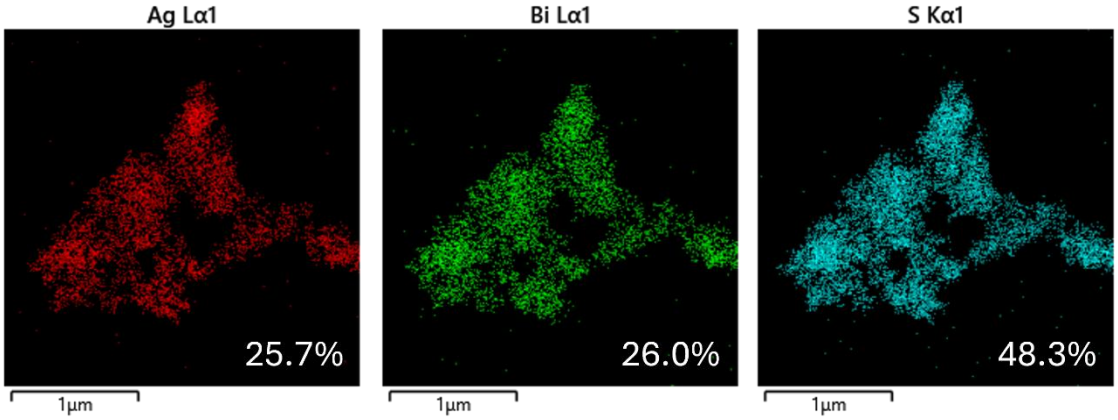

Figure S12. EDX mapping for $AgBiS_2$ nanocrystal sample prepared in equal parts oleylamine and octadecene at 200 °C, 1 h.

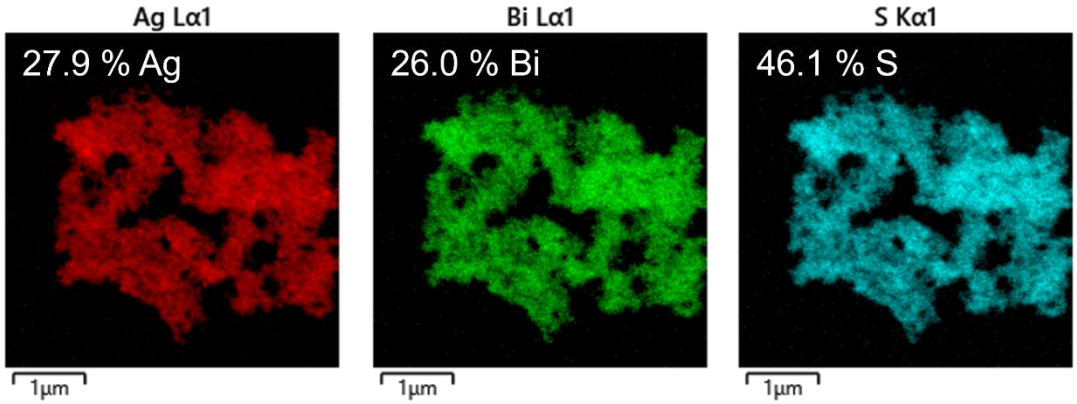

Figure S13. EDX mapping for $AgBiS_2$ nanocrystal sample prepared in oleylamine at 70 °C (60 minutes) with 2 equivalents of diethylammonium N,N-diethyldithiocarbamate added (0.4 mmol, 0.08 g).

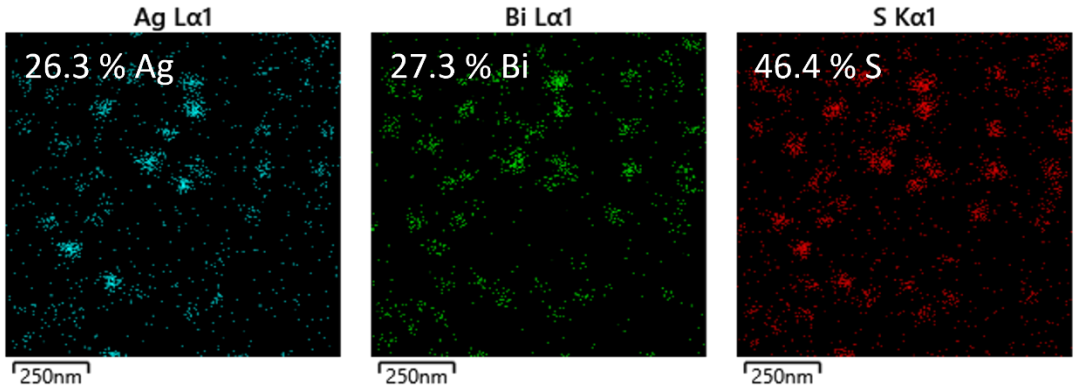

Figure S14. EDX mapping of $AgBiS_2$ nanocrystal sample prepared in oleylamine at 70 °C (60 minutes) with 2 equivalents of CS_2 added.

V. NMR reference spectra of solvents (oleylamine and dodecanethiol)

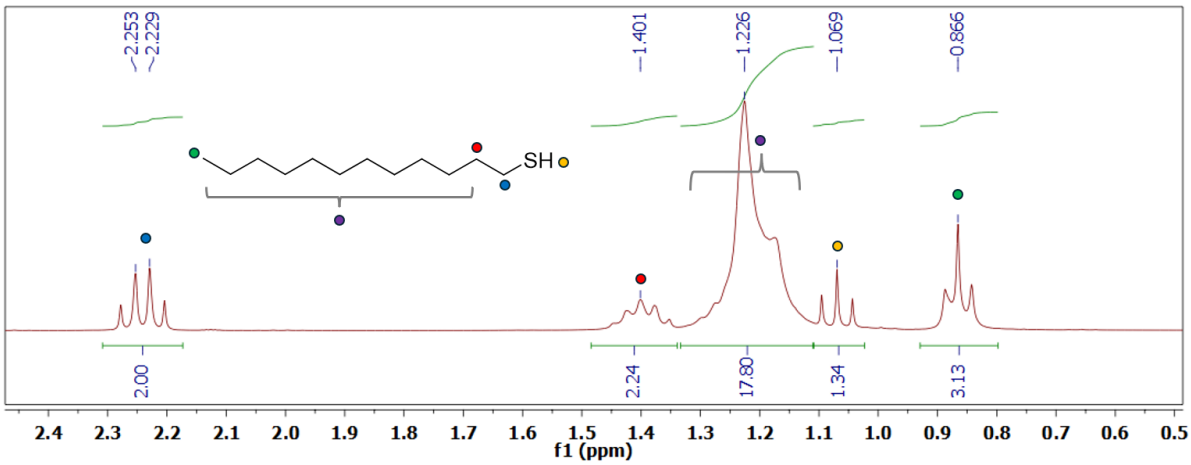

Figure S15. Reference ^{1}H NMR spectrum (d_8-toluene, 300 MHz, 25 °C) of dodecanethiol, with assignments for peaks.

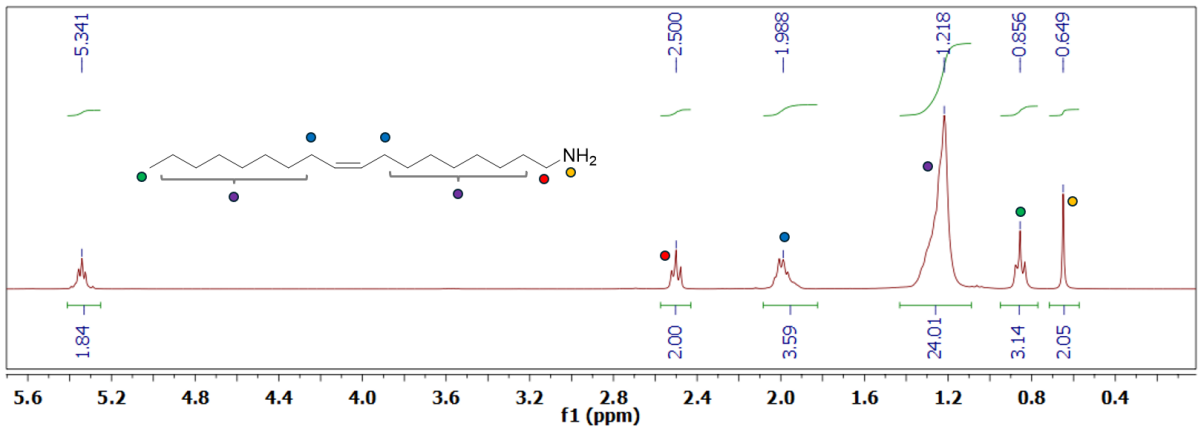

Figure S16. Reference ^{1}H NMR spectrum (d_8-toluene, 300 MHz, 25 °C) of oleylamine with assignments for peaks.

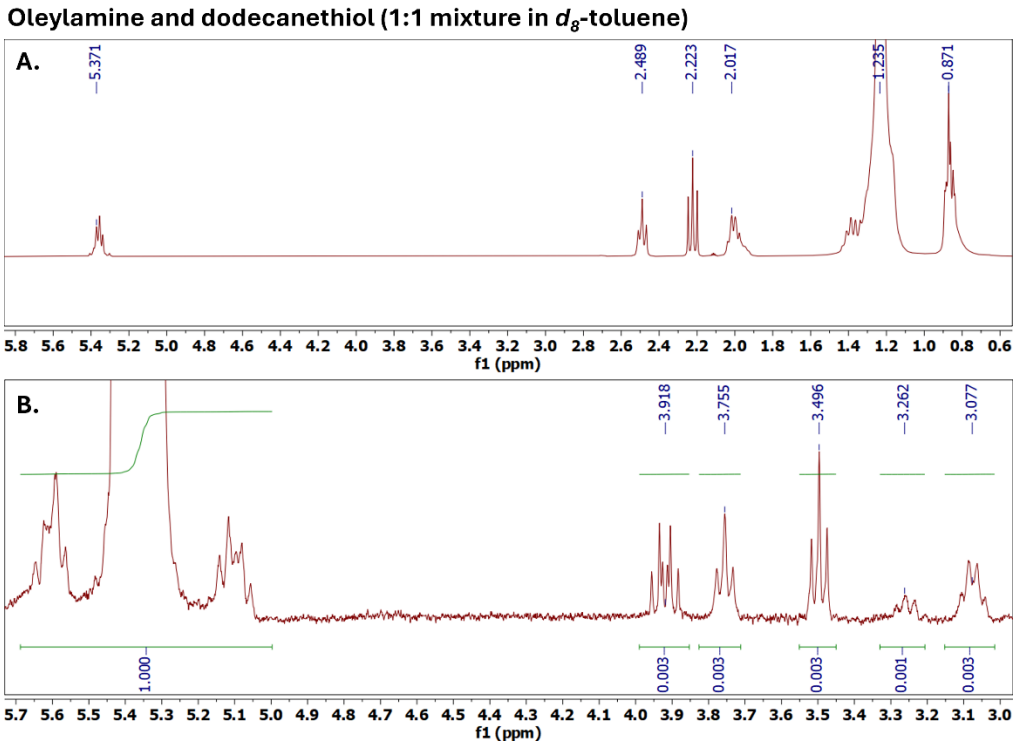

Figure S17. Reference ^{1}H NMR spectrum (d_8-toluene, 300 MHz, 25 °C) of an equimolar mixture of oleylamine and dodecanethiol, in a 50% by volume solution with d_8-toluene (the same solvent mixture used for NMR studies of precursor decomposition below). Panel A shows the full range of observed peaks from OLA/DDT. The shift of the amine -NH_2 peak (now overlapping with the terminal methyl groups at ~0.87 ppm) and shift/disappearance of the thiol -SH peak, as well as small shifts in the positions of protons on carbons adjacent to the amine and thiol functional groups, are consistent with the establishment of a proton transfer equilibrium between OLA and DDT. Panel B shows a magnified view of the region from 3.0 – 5.7 ppm, with the vertical scale greatly increased; this includes the region that is primarily studied to track precursor decomposition below. In this magnified view, various species that are present as small impurities in the solvent can now be observed. Integration relative to the oleylamine vinyl peak suggests that, in aggregate, these impurities account for on the order of 1% of the solvent.

VI. Preparation and NMR spectra of oleylammonium N-oleyldithiocarbamate

Synthesis of oleylammonium N-oleyldithiocarbamate. Carbon disulfide (5 mmol, 0.3 mL) was added dropwise to a solution of oleylamine (10 mmol, 3.27 mL) in diethyl ether (50 mL) at room temperature, leading to the formation of a white precipitate. The reaction mixture was dried *in vacuo*, giving the product as a white powder. ^{1}H NMR (300 MHz, $CDCl_3$, 25 °C; see Figure S18 for peak assignments): δ 7.62 (1H, t, J = 5 Hz), 6.92 (3H, br s), 5.35 (4H, m), 3.56 (2H, m), 3.06 (2H, t, J = 7 Hz), 2.02 (8H, m), 1.74 (2H, m), 1.59 (2H, m), 1.4 – 1.2 (44H, m), 0.89 (6H, m) ppm. ^{13}C NMR (126 MHz, $CDCl_3$, 25 °C; see Figure S18 for peak assignments): δ 211.9, 130.15, 130.12, 129.90, 129.86, 48.2, 40.6, 32.6, 31.9, 29.8 – 29.2 (multiple overlapping s), 28.8, 27.2, 27.1, 26.7, 22.7, 14.1 ppm.

Scheme S1. Synthesis of oleylammonium N-oleyldithiocarbamate.

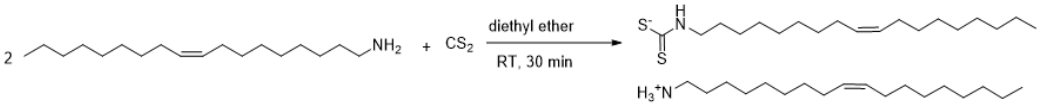

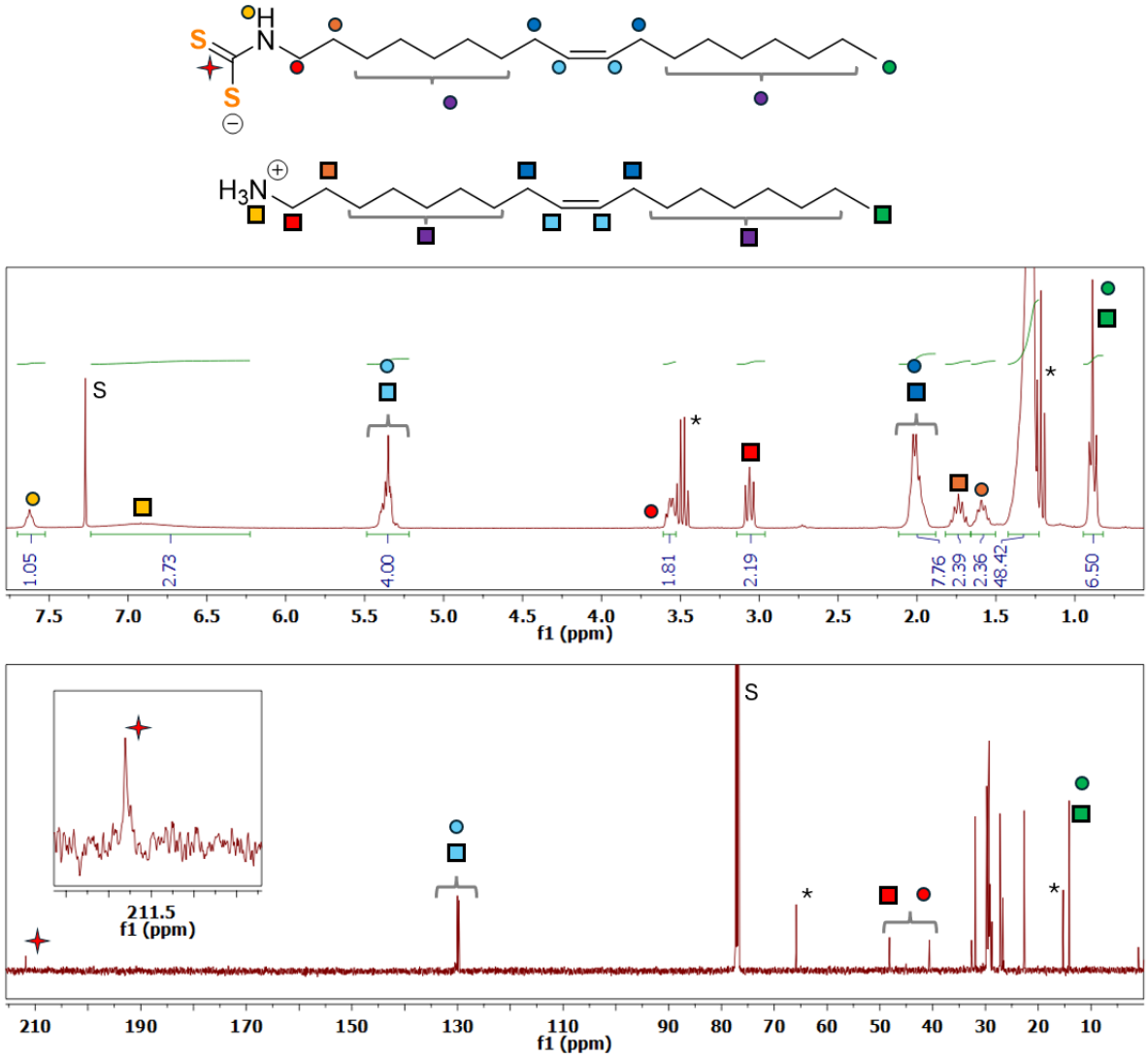

Figure S18. ^{1}H NMR (top, 300 MHz, $CDCl_3$, 25 °C) and ^{13}C NMR (bottom, 125 MHz, $CDCl_3$, 25 °C) of oleylammonium N-oleyldithiocarbamate prepared as described above. Peak assignments are indicated by colored circles (for the dithiocarbamate anion) and squares (for the oleylammonium cation); peak assignments are corroborated by ^{1}H-^{1}H COSY data, see Figure S19. * = residual Et_2O; S = $CDCl_3$ and residual $CHCl_3$.

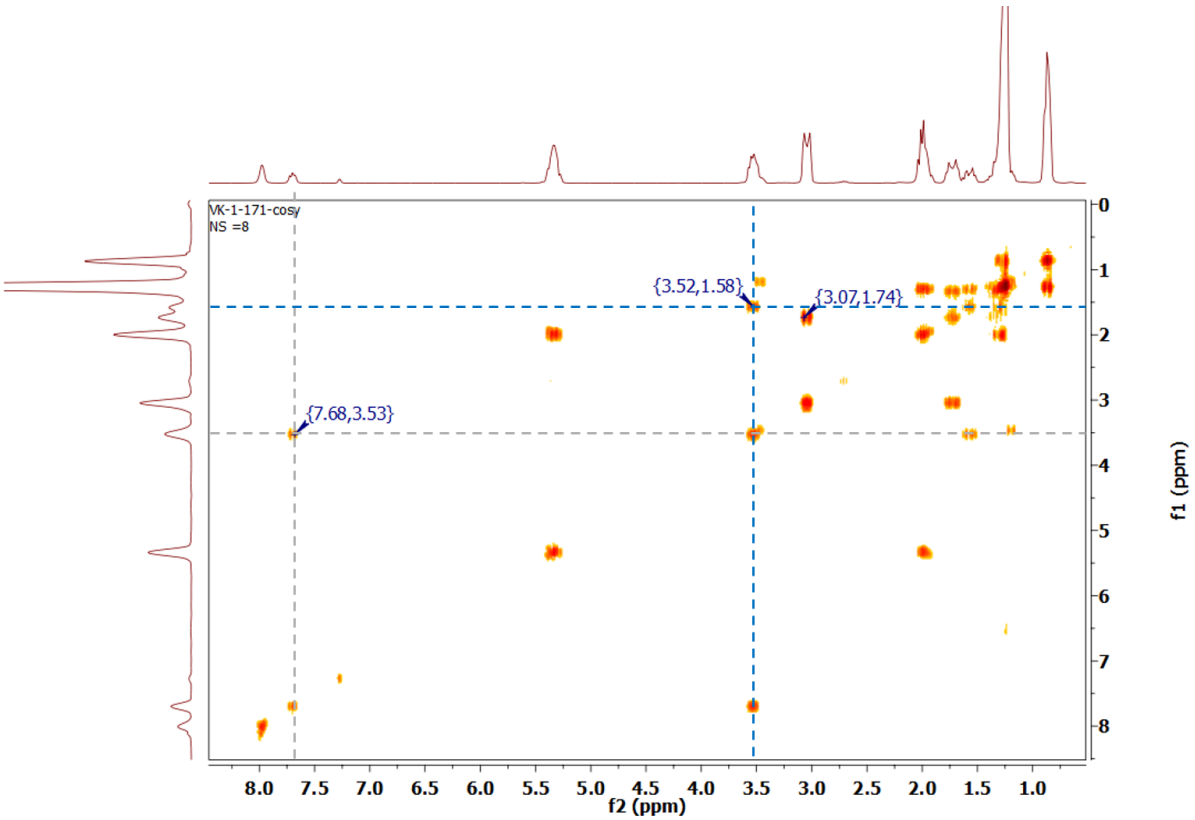

Figure S19. ^{1}H-^{1}H COSY data for oleylammonium N-oleyldithiocarbamate (500 MHz, room temperature, $CDCl_3$). The dashed lines highlight the coupling of the α protons (-NC*H*$_2$-) of the oleyldithiocarbamate group to the N*H* proton (at 7.7 ppm) as well as to the β protons of the N-oleyl group. No coupling is observed between the oleylammonium α protons and the N*H*$_3$ ammonium protons (at 8.0 ppm), presumably due to fast exchange on the NMR timescale; the cross-peak for coupling between the oleylammonium α and β protons is also labeled.

VII. Preparation and NMR spectra of N,N'-dioleylthiourea

Preparation of N,N'-dioleylthiourea. In a 50 mL round-bottom flask, 4.46 grams (16.7 mmol) of oleylamine ($C_{18}H_{37}N$) were carefully combined with 30 mL of toluene, accompanied by the gradual addition of 0.5 mL of carbon disulfide (CS_2). The mixture was gently stirred at a controlled temperature of 60 °C for 6 hours, allowing for thorough interaction between the components. After the heating process, the mixture was allowed to cool, and the solvents were evaporated, resulting in the formation of a white solid precipitate. ^{1}H NMR (500 MHz, $CDCl_3$, 25 °C; see Figure S20 for peak assignments): δ 5.65 (2H, br s), 5.35 (4H, m), 2.01 (8H, m), 1.60 (4H, m), 1.40 – 1.24 (44H, m), 0.88 (6H, t, *J* = 7 Hz) ppm. ^{13}C NMR (126 MHz, $CDCl_3$, 25 °C; see Figure S20 for peak assignments): δ 181.4, 130.0, 129.7, 44.4, 32.6, 31.9, 29.8 – 29.0 (multiple overlapping singlets), 27.2, 27.2, 26.9, 22.7, 14.1 ppm.

Scheme S2. Synthesis of N,N'-dioleylthiourea (RNH_2 = oleylamine).

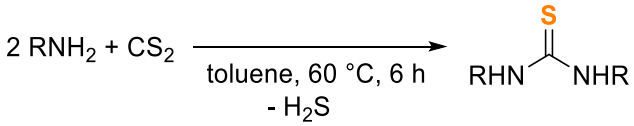

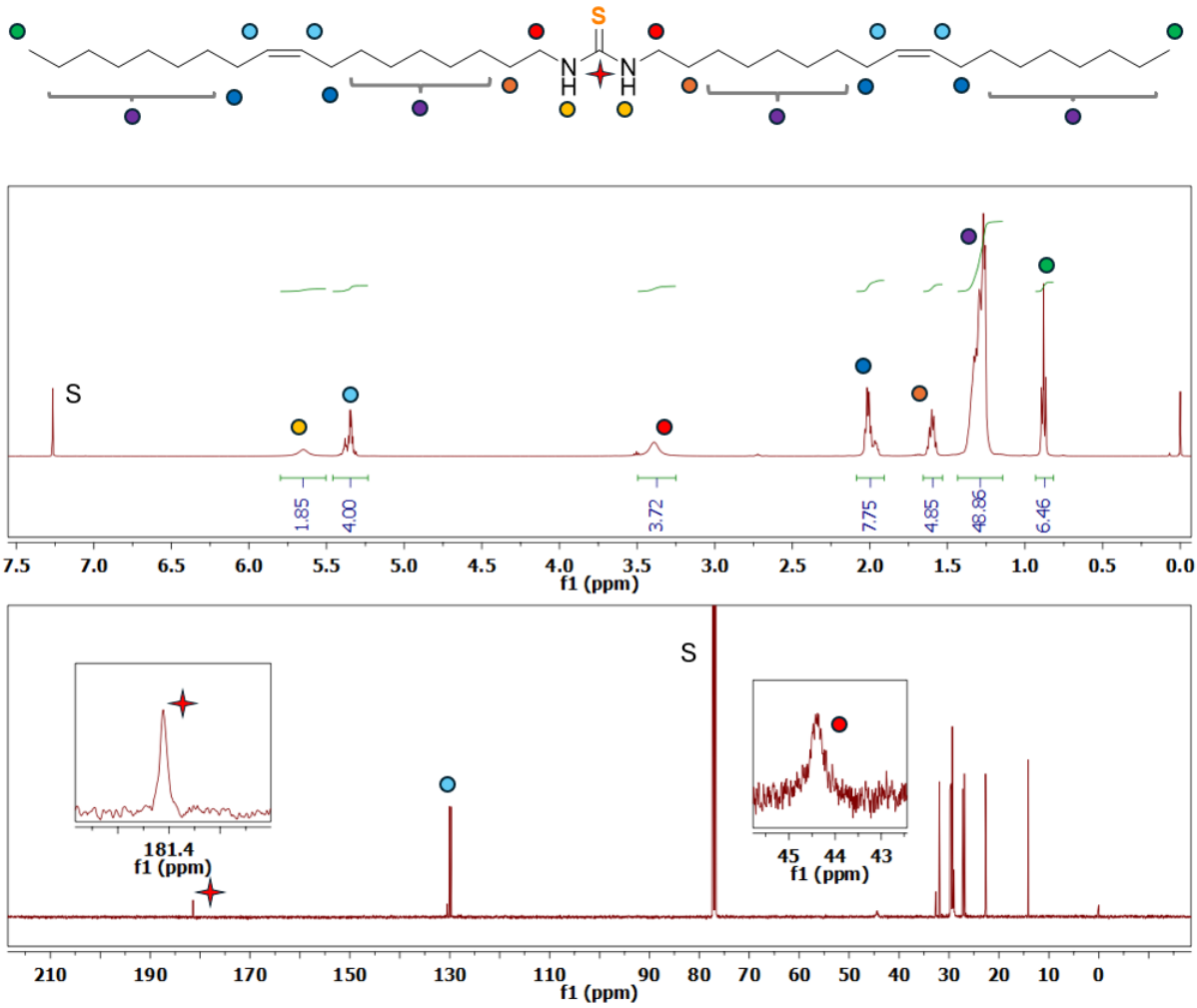

Figure S20. ^{1}H NMR (top, 500 MHz, $CDCl_3$, 25 °C) and ^{13}C NMR (bottom, 125 MHz, $CDCl_3$, 25 °C) of N,N'-dioleylthiourea prepared as described above. Peak assignments are indicated by colored circles. S = $CDCl_3$ and residual $CHCl_3$.

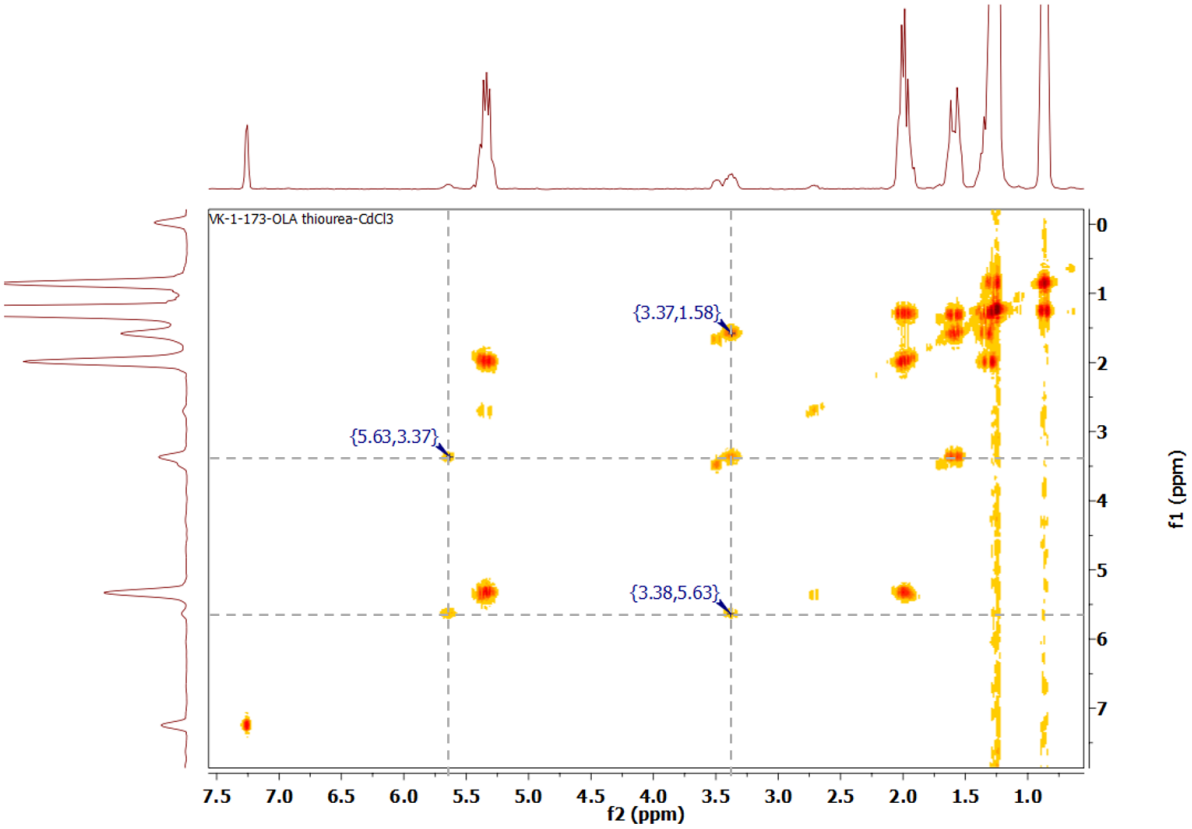

Figure S21. ^{1}H-^{1}H COSY data for N,N'-dioleylthiourea (300 MHz, room temperature, $CDCl_3$). The dashed lines highlight the crosspeaks for the coupling of the α protons (-NC*H*$_2$-) of the oleyl groups to the N*H* proton (at 5.63 ppm); note that this coupling is not readily apparent in the one-dimensional ^{1}H spectrum due to broadening of the peaks.

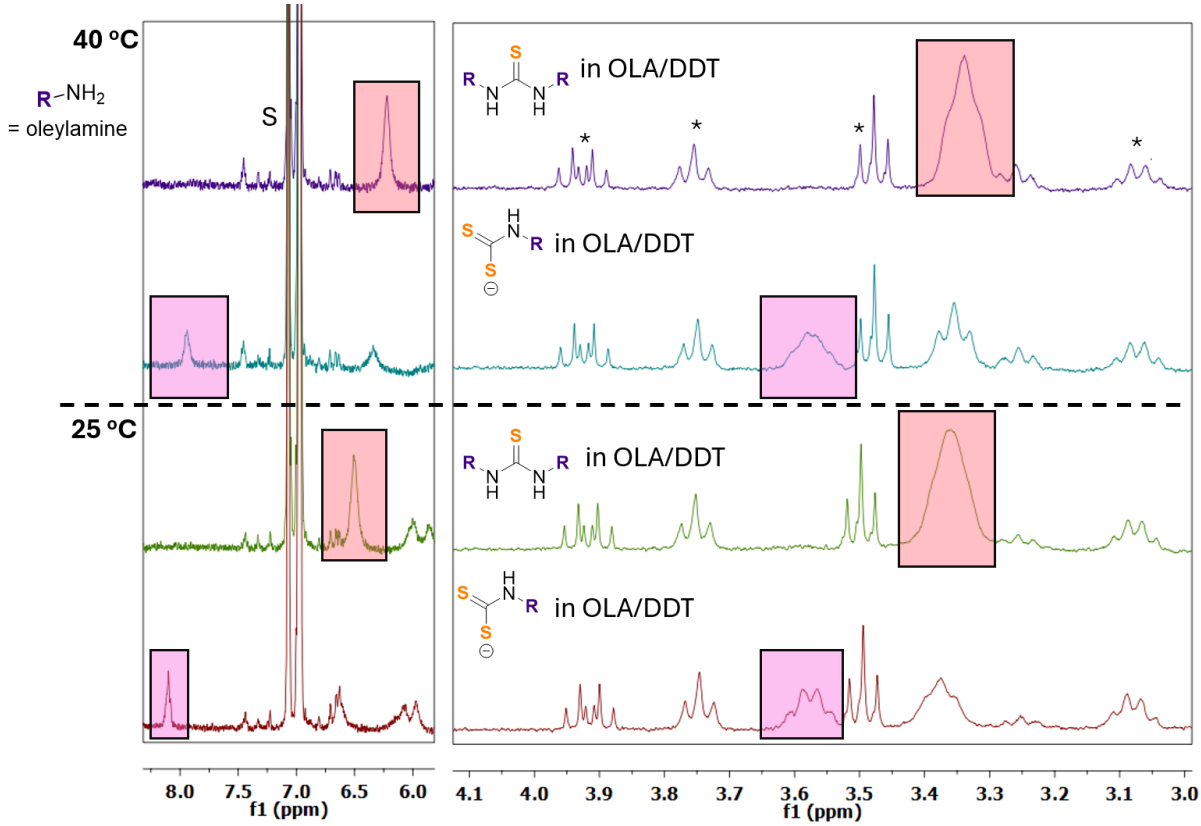

Figure S22. Reference ^{1}H NMR spectra (300 MHz, d_8-toluene) of N,N'-dioleylthiourea and N-oleyldithiocarbamate in oleylamine and dodecanethiol at 40 °C and 25 °C. The samples were prepared using an equimolar mixture of oleylamine and dodecanethiol which was then diluted 1:1 (by volume) with d_8-toluene, to match the solvent environment used for the decomposition experiments shown below. The peaks highlighted in purple and orange were those used to identify the formation of N,N'-dioleylthiourea and N-oleyldithiocarbamate (respectively) in the NMR decomposition experiments. Note that there is an impurity of the N,N'-dioleylthiourea present in the N-oleyldithiocarbamate sample due to the instability of the latter compound which decomposes to the thiourea upon storage (see Figure S23). Peaks attributed to solvent impurities are marked with a * in the top spectrum and peaks from residual C_7D_7H are marked with S in the top spectrum.

VIII. NMR spectra of N-oleyldithiocarbamate in the presence of $Bi(NO_3)_2$

Oleyldithiocarbamate binding to bismuth. In order to observe the spectral changes that might be expected upon interaction of the oleyldithiocarbamate formed *in situ* and the metal ions, oleylammonium N-oleyldithiocarbamate as combined with bismuth(III) nitrate in a 3:1 ratio in acetone, stirred at room temperature, then concentrated to dryness *in vacuo* (Scheme S3). No further purification was attempted on this material; therefore, the expected byproduct oleylammonium nitrate is also present. The resulting NMR spectrum in $CDCl_3$ is shown in Figure S23 in comparison to oleylammonium N-oleyldithiocarbamate. This spectrum also shows that the oleyldithiocarbamate material, after storage at room temperature for several days, shows partial degradation to give N,N'-dioleylthiourea (compare to Figure S22).

Scheme S3. Combination of oleylammonium N-oleyldithiocarbamate with bismuth nitrate.

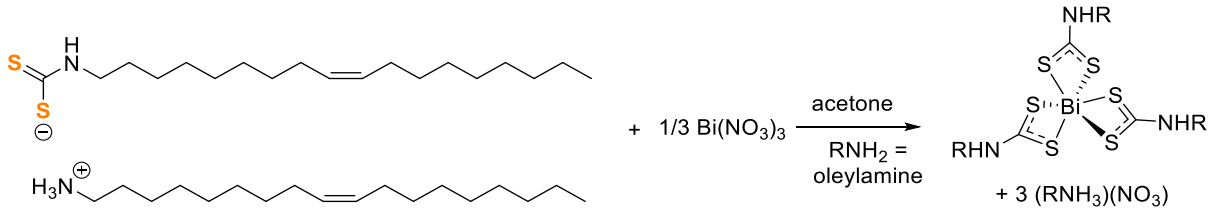

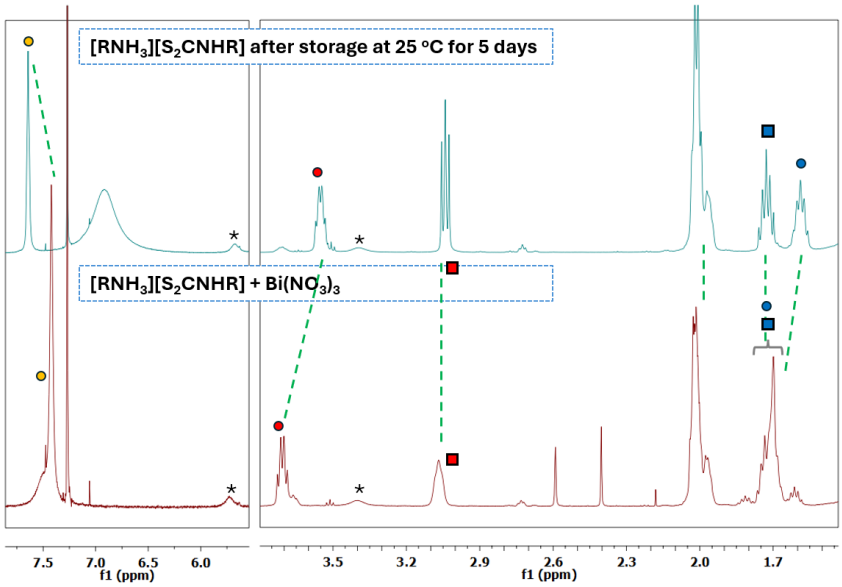

Figure S23. ^{1}H NMR (500 MHz, $CDCl_3$, 25 °C) of (top) oleylammonium N-oleyldithiocarbamate after storage at room temperature for five days, showing the appearance of peaks (marked with *) corresponding to N,N'-dioleylthiourea. (Bottom) Spectrum of the species produced by combining oleylammonium N-oleyldithiocarbamate with bismuth nitrate. Peaks are marked with colored circles/squares according to the assignment shown above in Figure S18. The most significant shifts are observed for the dithiocarbamate N*H* and N-C*H*$_2$- signals due to binding to Bi^{3+}.

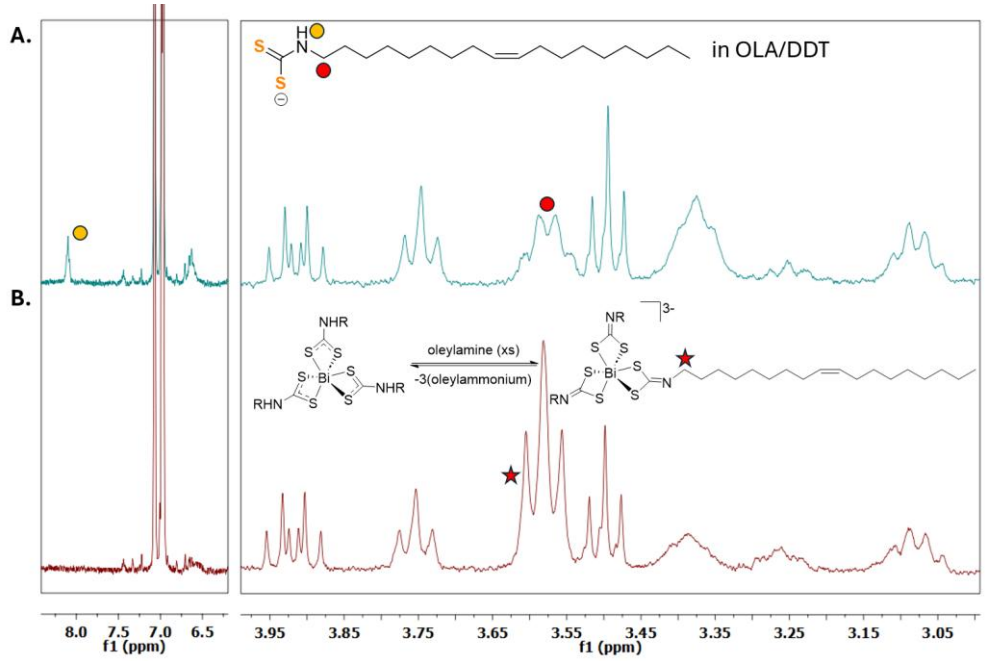

Figure S24. Comparison of the ^{1}H NMR spectrum (300 MHz, d_8-toluene/oleylamine/dodecanethiol, room temperature) of N-oleyldithiocarbamate (A, as shown previously in Figure S22) and the putative bismuth tris(N-oleyldithiocarbamate) complex prepared as described above (B). Notably, when the complex is dissolved in excess oleylamine/dodecanethiol, the signal for the N-H proton of the dithiocarbamate ligands and the quartet signal for the α-NCH_2 protons of the dithiocarbamate ligands, both of which were observed in the spectrum of this species in the absence of excess oleylamine (see Figure S23), disappear. In place of the latter, a new triplet signal is observed, which we also observed in our NMR decomposition studies of the bismuth diethyldithiocarbamate complex under these conditions. These observations are attributed to the deprotonation of the dithiocarbamate N-H in the presence of excess oleylamine base as illustrated in part (B).

IX. Variable-temperature NMR spectra of $[H_2NEt_2][S_2CNEt_2]$ in the presence of oleylamine or oleylamine and dodecanethiol

Diethylammonium N,N-diethyldithiocarbamate was prepared as previously reported and recrystallized from diethyl ether.[3] The solutions for NMR analysis were prepared by stirring 0.2 mmol of $[H_2NEt_2][S_2CNEt_2]$ in either 9 mmol of oleylamine or 9 mmol each of oleylamine and dodecanethiol, and the mixture was stirred at room temperature under vacuum for 30 minutes. A 300 µL aliquot of this mixture was then mixed with 300 µL of d_8-toluene in an NMR tube. The sample was equilibrated at each temperature for approximately 15 minutes before the spectrum was acquired.

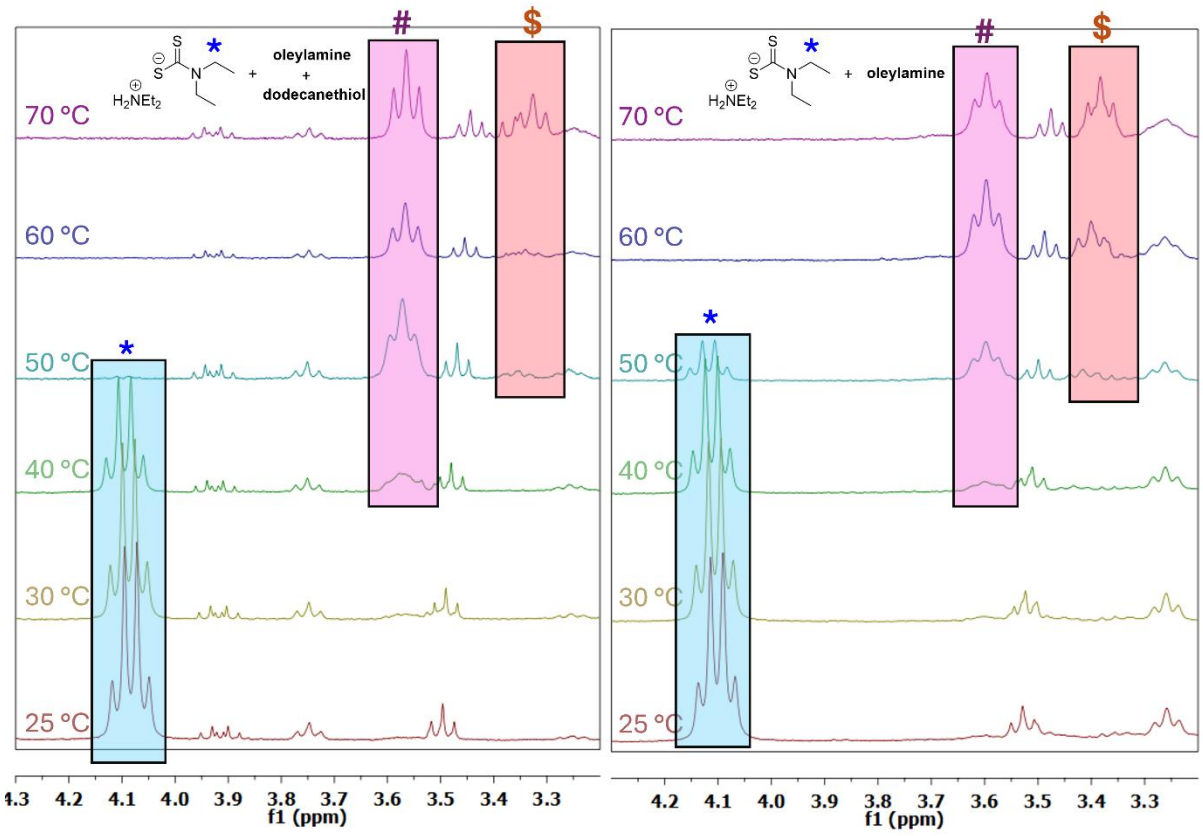

Figure S25. Comparison of the variable-temperature NMR data (^{1}H NMR, 300 MHz, in a 1:1 mixture of d_8-toluene and OLA and/or DDT) for diethylammonium diethyldithiocarbamate in a combination of oleylamine/dodecanethiol or in only oleylamine. The highlighted peaks correspond to the N-CH_2 protons of each species: blue (*) for the N,N-diethyldithiocarbamate, pink (#) for N-oleyldithiocarbamate, and orange ($) for N,N'-dioleylthiourea.

X. Variable temperature NMR spectra of $Bi(S_2CNEt_2)_3$ and $Ag(S_2CNEt_2)$ in oleylamine and/or dodecanethiol

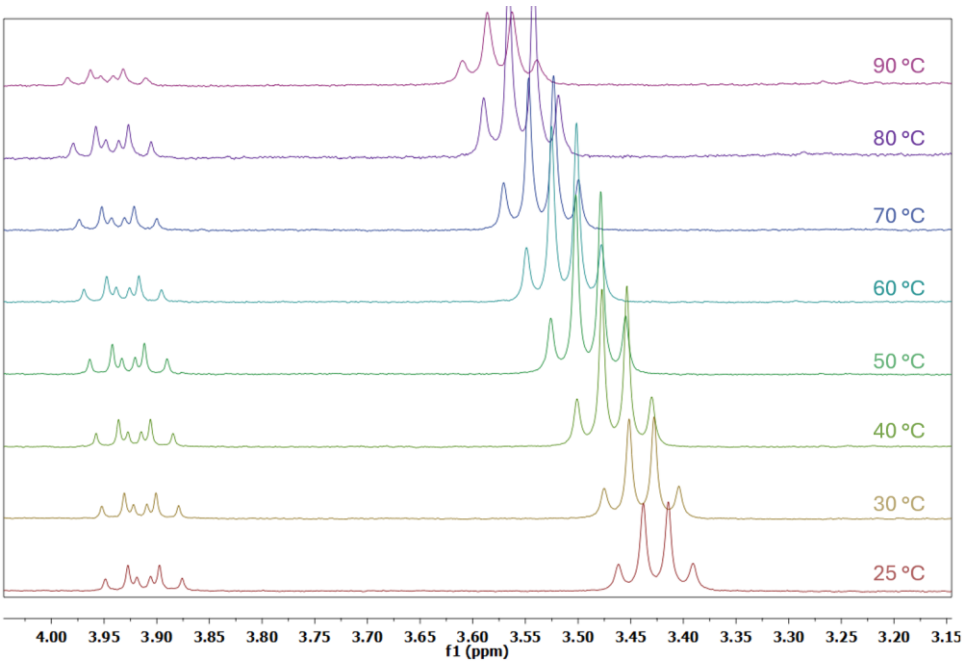

Figure S26. Variable-temperature ^{1}H NMR spectra (300 MHz, d_8-toluene) of $Ag(S_2CNEt_2)$ and $Bi(S_2CNEt_2)_3$ in the presence of dodecanethiol. The solution was prepared by combining 0.2 mmol each of the metal complexes to 18 mmol of dodecanethiol (4.2 mL); the mixture was stirred and sonicated at room temperature until the precursors fully dissolved. A 300 µL aliquot of this mixture was then mixed with 300 µL of d_8-toluene in an NMR tube. The sample was equilibrated at each temperature for 15 minutes before the spectrum was acquired.

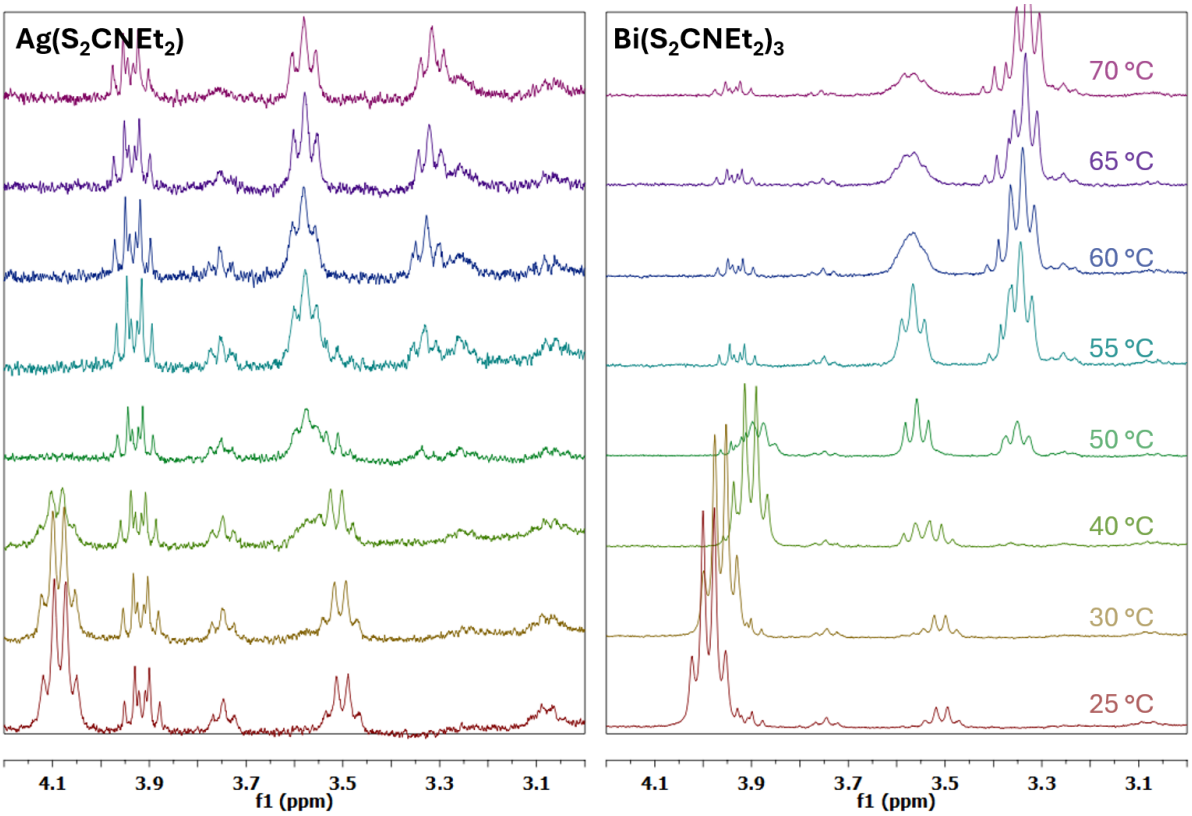

Figure S27. Variable-temperature ^{1}H NMR spectra (300 MHz, d_8-toluene) of $Ag(S_2CNEt_2)$ (left) and, separately, $Bi(S_2CNEt_2)_3$ (right) in the presence of dodecanethiol and oleylamine. Each solution was prepared by combining 0.2 mmol of the metal complexes to 9 mmol of dodecanethiol and 9 mmol of oleylamine; the mixture was stirred and sonicated at room temperature until the precursors fully dissolved. A 300 µL aliquot of this mixture was then mixed with 300 µL of d_8-toluene in an NMR tube. The sample was equilibrated at each temperature for 15 minutes before the spectrum was acquired.

XI. NMR spectra of NaS_2CNEt_2, $[H_2NEt_2][S_2CNEt_2]$, $[TBA][S_2CNEt_2]$, $Bi(S_2CNEt_2)_3$, and $Ag(S_2CNEt_2)$ at 40 °C over time in oleylamine or oleylamine and dodecanethiol

Unless otherwise stated, solutions for analysis shown in this section were prepared by dissolving 0.06 mmol (for $Bi(S_2CNEt_2)_3$) or 0.2 mmol (for other compounds) in either 3 mL of oleylamine or 3 mL of a 1:1 (mol:mol) mixture of oleylamine and dodecanethiol, which was stirred and sonicated at room temperature. A 300 µL aliquot of this mixture was then mixed with 300 µL of d_8-toluene in an NMR tube. The NMR tube was inserted into a pre-heated NMR instrument at 40 °C for analysis.

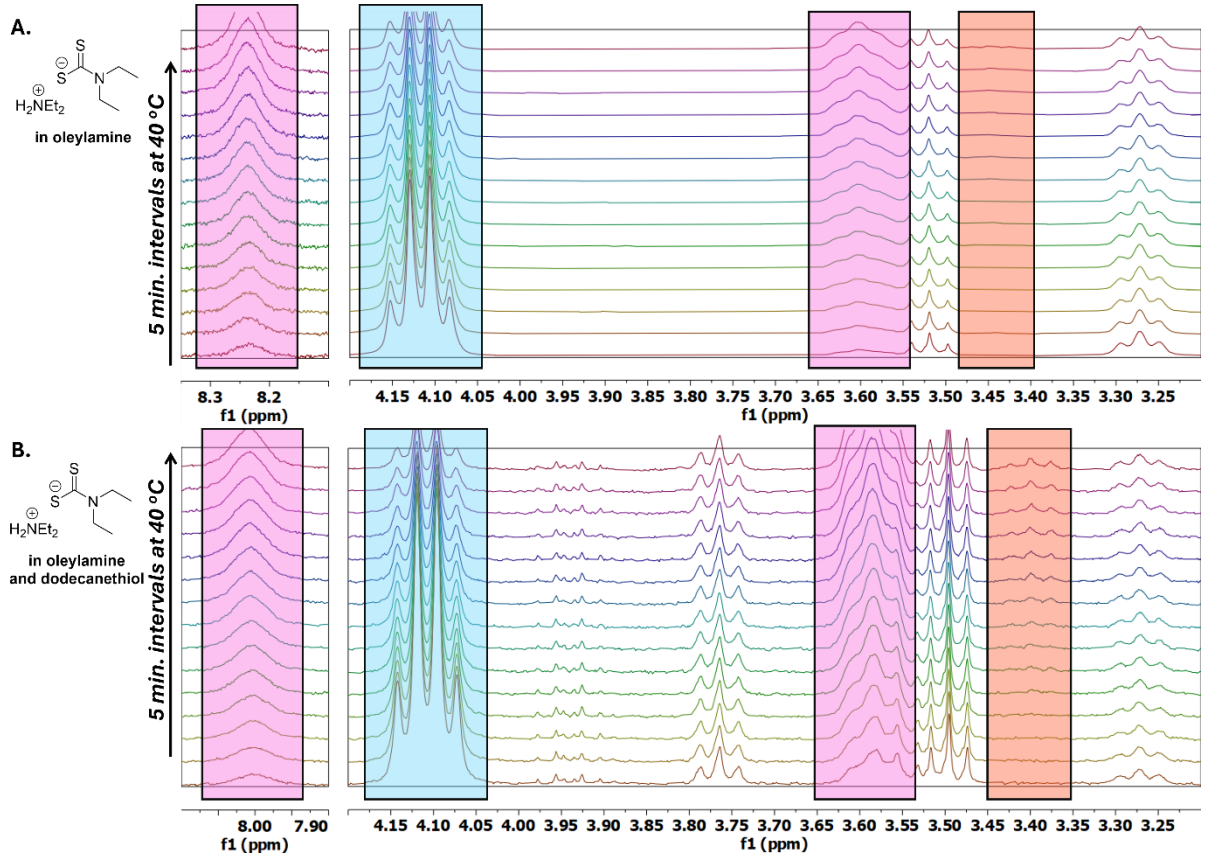

Figure S28. ^{1}H NMR (300 MHz, d_8-toluene) of diethylammonium N,N-diethyldithiocarbamate in the presence of (A) oleylamine or (B) oleylamine and dodecanethiol at 40 °C. Gradual decomposition of the dithiocarbamate (4.15 ppm, blue) is observed concomitant with growth of two new features (3.65 ppm and 8.05 ppm, pink) associated with N-oleyldithiocarbamate. More gradually an additional feature, attributed N,N'-dioleylthiourea, grows in at 3.38 ppm (orange). Other features remain unchanged over this temperature range and time and likely correspond to solvent impurities (see above).

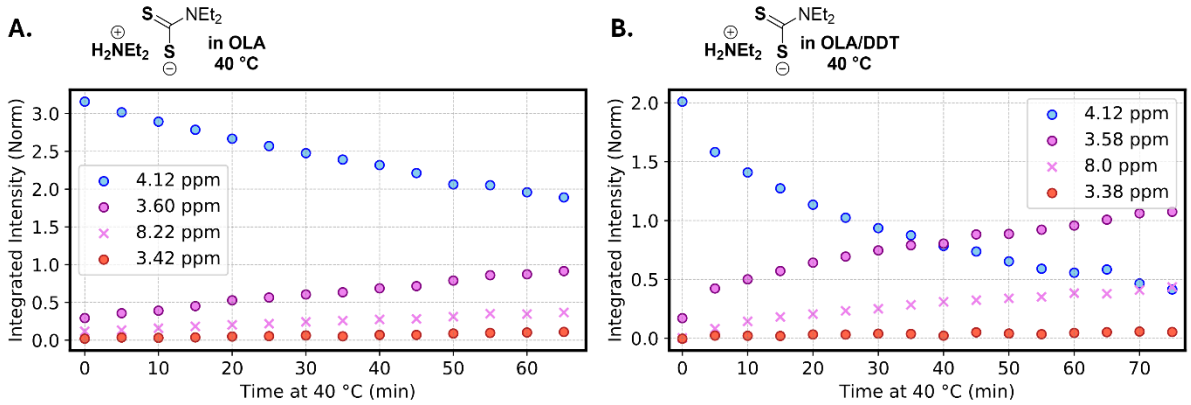

Figure S29. Relative integrals of the highlighted peaks in Figure S28 A and B, respectively.

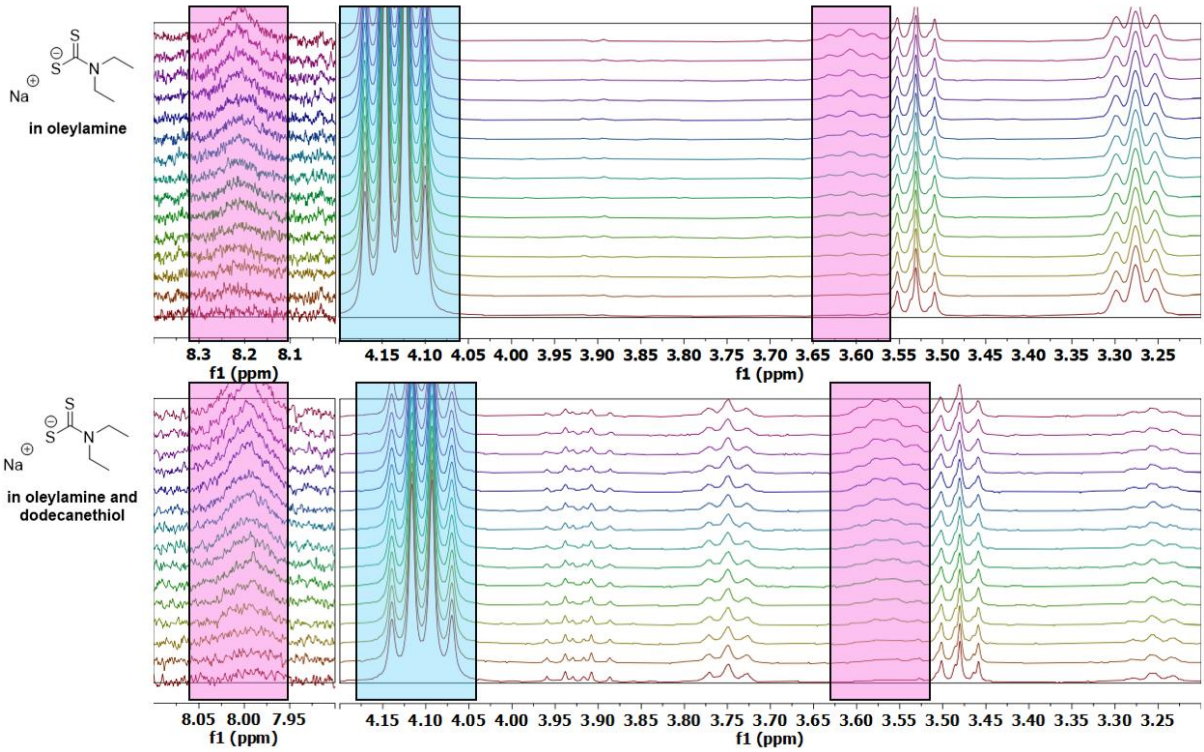

Figure S30. ^{1}H NMR (300 MHz, d_8-toluene) of sodium N,N-diethyldithiocarbamate in the presence of excess oleylamine (top) or oleylamine and dodecanethiol (bottom) at 40 °C. Solutions were stirred briefly under vacuum at room temperature before preparing the NMR sample. Gradual decomposition of the diethyldithiocarbamate (blue) is observed concomitant with growth of new features corresponding to N-oleyldithiocarbamate (pink). No formation of N,N'-dioleylthiourea is observable in this experiment (expected to give a triplet peak in the 3.30 – 3.40 ppm region). Other features observed in this region remain largely unchanged over this temperature range and time and may correspond to solvent impurities (see above).

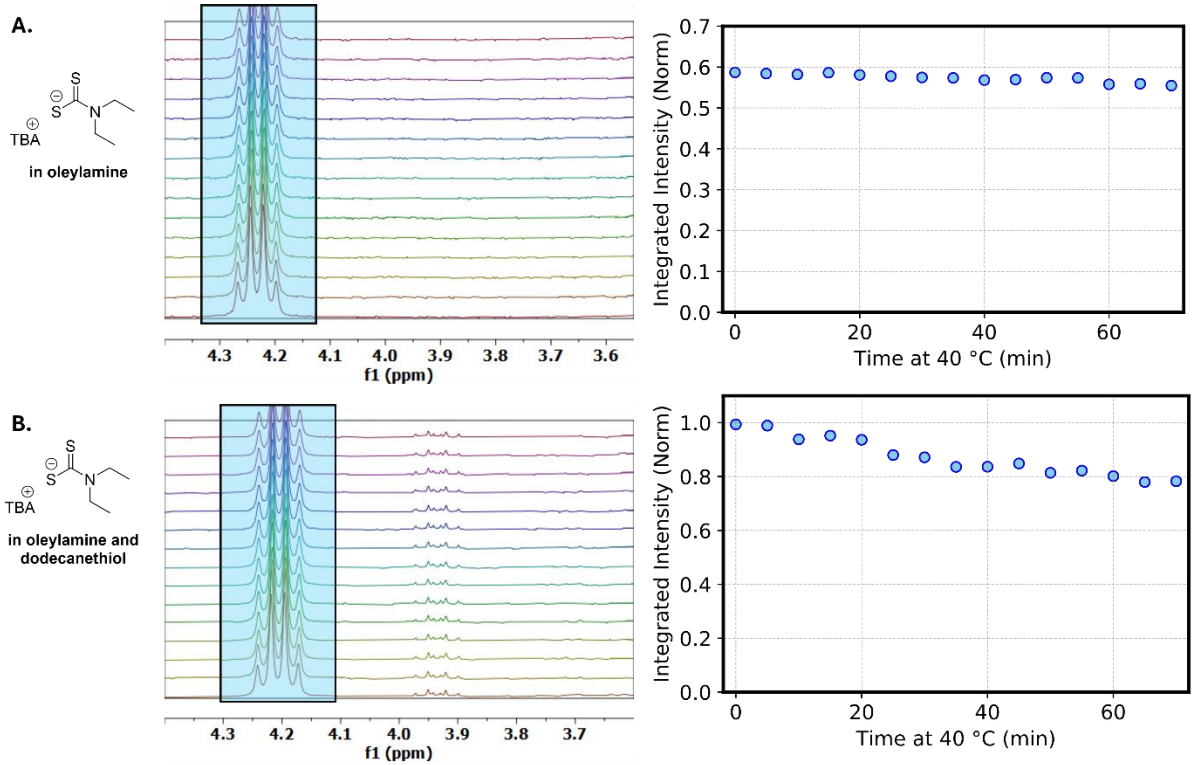

Figure S31. ^{1}H NMR (300 MHz, d_8-toluene) of tetrabutylammonium (TBA) N,N-diethyldithiocarbamate in the presence of excess (A) oleylamine, or (B) oleylamine and dodecanethiol at 40 °C. Solutions were stirred briefly under vacuum at room temperature before preparing the NMR sample. Gradual decomposition of the diethyldithiocarbamate (blue) is observed in (B), but essentially no change is observed in (A). [TBA][S_2CNEt_2] was prepared as previously reported and recrystallized from acetonitrile/ether.[4]

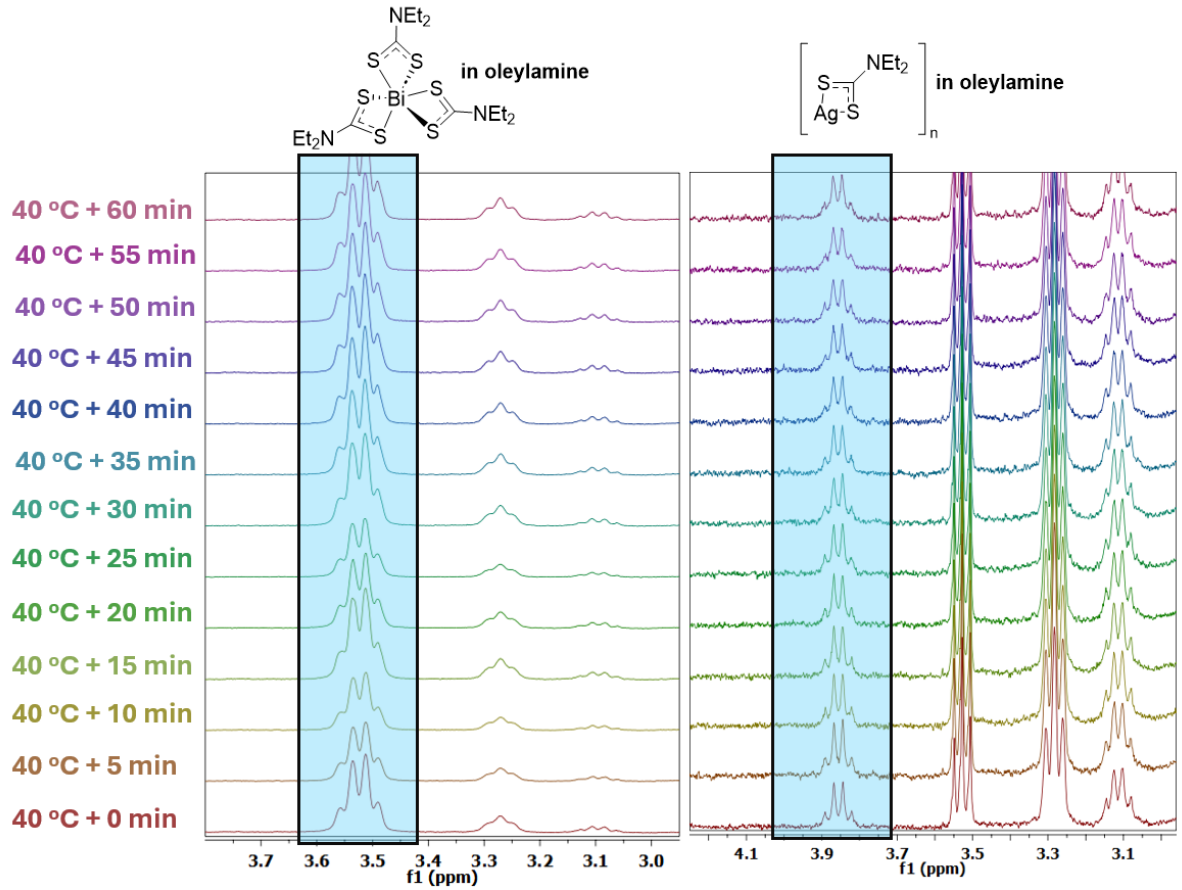

Figure S32. ^{1}H NMR (300 MHz, d_8-toluene) of $Bi(S_2CNEt_2)_3$ (left) and $Ag(S_2CNEt_2)$ (right) in oleylamine at 40 °C. The peak attributed to the N-CH_2CH$_3$ peaks of the $[S_2CNEt_2]^-$ ligands is highlighted in blue. No significant decomposition of the complexes is observed over the course of an hour at 40 °C. Note that the concentration of $Ag(S_2CNEt_2)$ is low because of its lower solubility in oleylamine alone at this temperature.

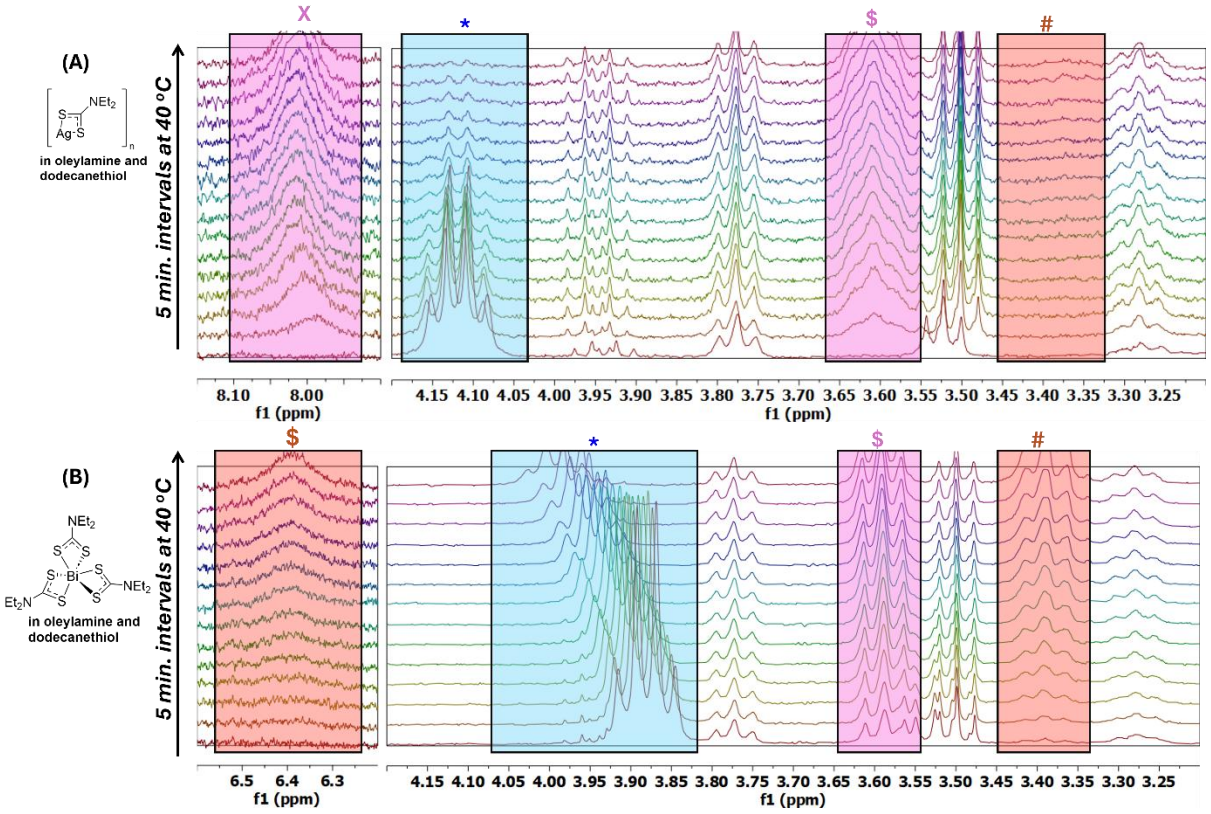

Figure S33. ^{1}H NMR (300 MHz, d_8-toluene) of $Ag(S_2CNEt_2)$ (A, top) and $Bi(S_2CNEt_2)_3$ (B, bottom) in oleylamine and dodecanethiol. The bottom spectrum in each case shows the sample at room temperature before heating and the next spectrum shows the first data point acquired at 40 °C; subsequent spectra were taken at the given times after the first 40 °C spectrum. The peaks attributed to the N-CH_2CH$_3$ protons of the $[S_2CNEt_2]^-$ ligands are highlighted in blue, which decrease in intensity with time. In (A), the peaks (pink) corresponding to N-oleyldithiocarbamate grow in. In (B), the triplet growing in at 3.60 ppm combined with the lack of a peak near 8.00 ppm, is more consistent with a deprotonated N-oleyldithiocarbiminate ligand (see Scheme S4), suggesting facile deprotonation of the bismuth-bound primary dithiocarbamate. Subsequently, N,N'-dioleylthiourea grows in (orange). Symbols in the figure correspond to assignments shown in Scheme S4.

Scheme S4. Reactions representing the transformations in the NMR experiments shown in Figure S33.

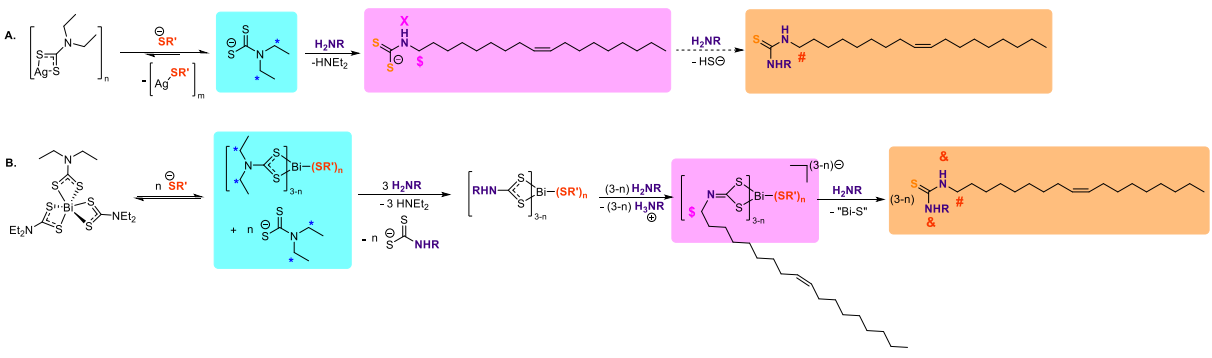

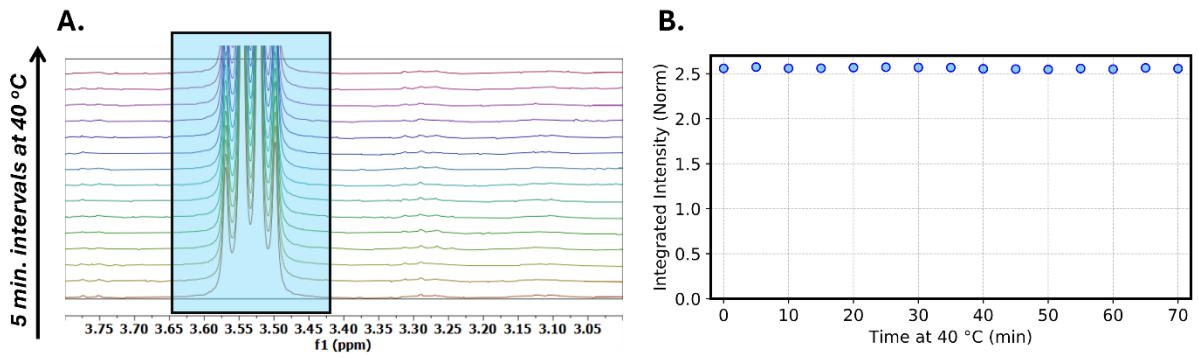

Figure S34. (A) ^{1}H NMR spectra (300 MHz, d_8-toluene, 40 °C) of $Bi(S_2CNEt_2)_3$ in oleylamine with one equivalent of triflic acid (TfOH). To prepare the sample, triflic acid was added to oleylamine before $Bi(S_2CNEt_2)_3$ was added, then the sample was prepared as described in the general procedure at the beginning of this section. The highlighted peak corresponds to the α N-CH_2 protons of the ethyl groups. (B) shows the relative integral of this peak over time at 40 °C.

XII. Mechanistic hypotheses in the presence of CS_2

Scheme S5. Possible pathways involved in reaction with added CS_2

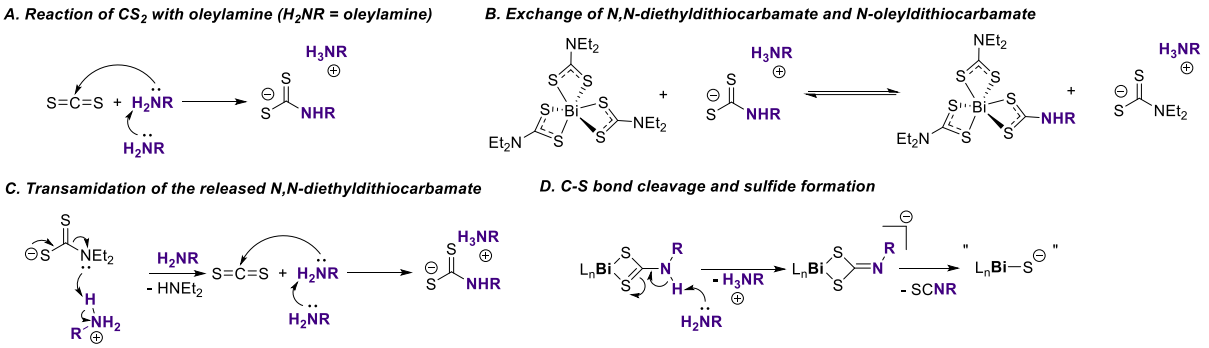

Scheme S5 shows the pathways we hypothesize to be involved in precursor conversion when CS_2 is added to the reaction mixture. In (A), the known reaction of CS_2 with oleylamine to give N-oleyldithiocarbamate is shown. As shown in B, this can exchange with the N,N-diethyldithiocarbamate ligands on bismuth (or silver), which our NMR studies show are easily exchangeable in the presence of additional coordinating ligands. This exchange releases one of the bound N,N-diethyldithiocarbamates as the oleylammonium salt. The oleylammonium cation acts as an acid source to promote transamidation of the N,N-diethyldithiocarbamate, as shown in (C). The N-oleyldithiocarbamate formed in (C) can again bind to the metal as shown in (B). In (D), the bound N-oleyldithiocarbamate decomposes further to release sulfide. Note that steps (C) and (D) are the same as shown for the general case in Scheme 4A(ii-iii) of the main text.

It is important to note that CS_2 not only acts as a direct source of N-oleyldithiocarbamate, but also, through this process, generates an equivalent of acid which acts to catalyze the transamidation of the N,N-diethyldithiocarbamate. Therefore, only catalytic amounts of CS_2 are in principle necessary to accelerate the overall precursor conversion reaction. Further investigation of this process to confirm this hypothesis is ongoing.

XIII. UV-vis-NIR spectra

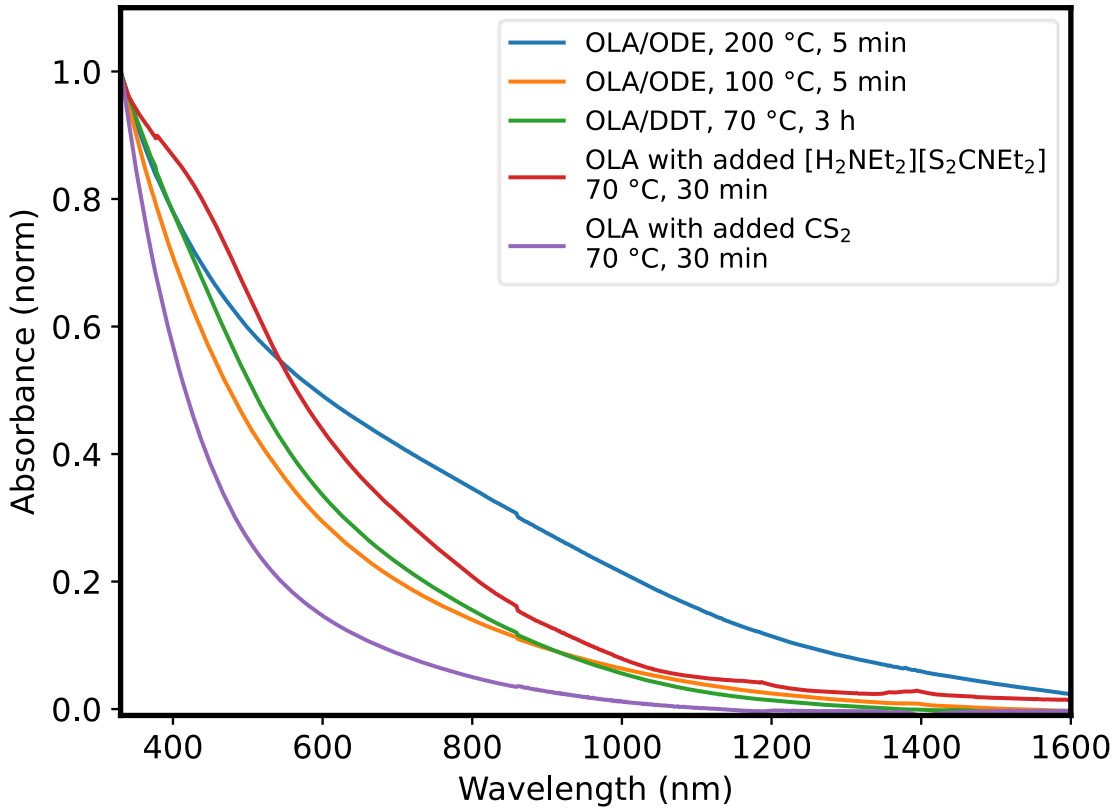

Figure S35. UV-Vis spectra of $AgBiS_2$ particles (suspended in toluene) prepared under different conditions (as described in the legend). Spectra were normalized at 370 nm to facilitate comparison.

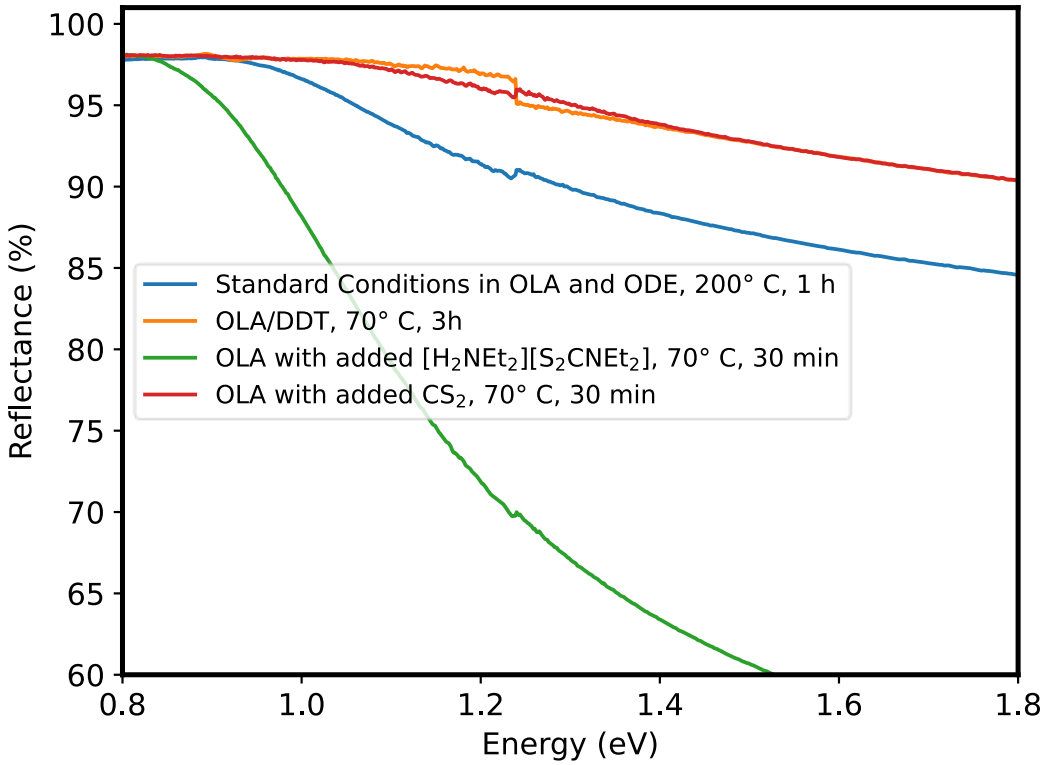

Figure S36. Diffuse reflectance spectra for selected $AgBiS_2$ nanocrystal samples, prepared with the conditions stated in the legend. Data is unscaled and different absolute reflectance values result from different sample concentrations (samples were mixed with reference material before acquisition).

The diffuse reflectance data was analyzed using the Kubelka-Munk transformation to estimate the optical band gap. The following equation gives the relation between reflectance data and the Kubelka-Munk function F(R)[5–7]:

$$F(R) = (1 - R)^2/2R$$

where $F(R)$ is the Kubelka-Munk function and R is the absolute reflectance.

Since $AgBiS_2$ is known to be an indirect bandgap material, an appropriate Tauc analysis was carried out on each sample by plotting $(F(R)\cdot h\nu)^{1/2}$, where h is Planck's constant and ν is the photon frequency. A fit to the linear region above the absorption onset was performed and the energy position of the intercept of this line with a linear fit to the low-energy (sub-bandgap) baseline is taken as the indirect band gap.[6–9]

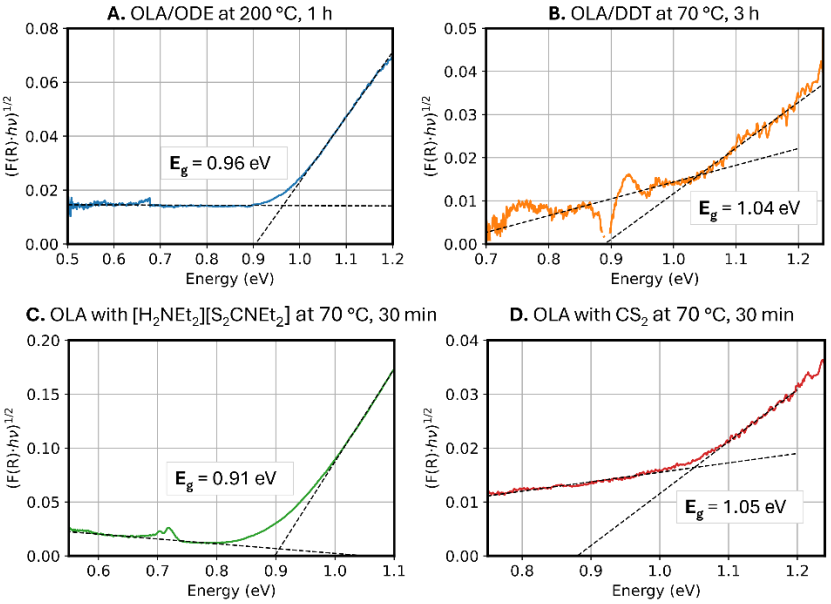

Figure S37. Determination of the indirect band gap (E_g) by Tauc analysis for selected $AgBiS_2$ samples prepared under different conditions.

XIV. Additional Computational Results and Discussion

Table S2. DFT-computed absolute isotropic shielding for α-protons (N-C*H*$_2$CH$_3$) protons of N,N-diethyldithiocarbamate in the free ion and in bismuth and silver complexes

		Calculated Shieldings[a]				Average Shielding[b]	Average Shift[c]
	Species	**H_a**	**H_b**	**$H_{a'}$**	**$H_{b'}$**		
(A)	$[S_2CNEt_2]^-$	26.45	28.89	26.45	28.89	27.67	3.45
(B)	$Ag[S_2CNEt_2]$	27.49	28.44	27.49	28.44	27.97	3.16
(C)	$Ag(S_2CNEt_2)(NH_2Bu)$	27.40	28.43	27.15	28.60	27.90	3.23
(D)	$Bi[S_2CNEt_2]_3$	27.23	28.43	27.14	28.46	27.82	3.31
	TMS	31.12					
(A)	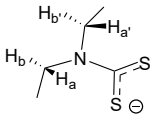						
(B)	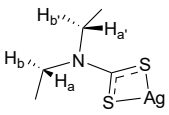						
(C)	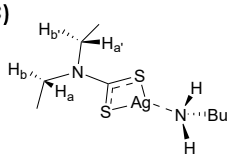						
(D)	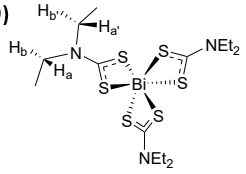						

[a]Calculated without spin-spin coupling at the B3LYP/def2svp level of theory [b]Chemical shielding is given in ppm [c]Chemical shift is given in ppm relative to tetramethylsilane (TMS)

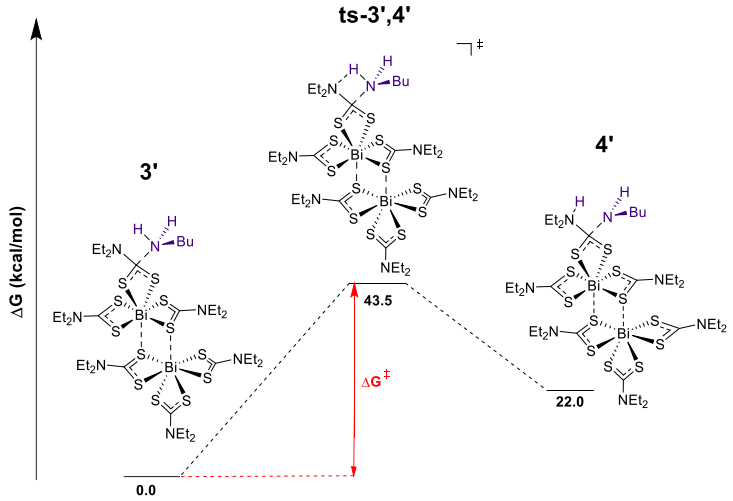

Figure S38. Reaction coordinate diagram for the direct transamidation for N,N-diethyldithiocarbamate coordinated to Bi^{3+} as part of the $[Bi(S_2CNEt_2)_3]_2$ dimer, based on the reported crystal structure of this species.[10]

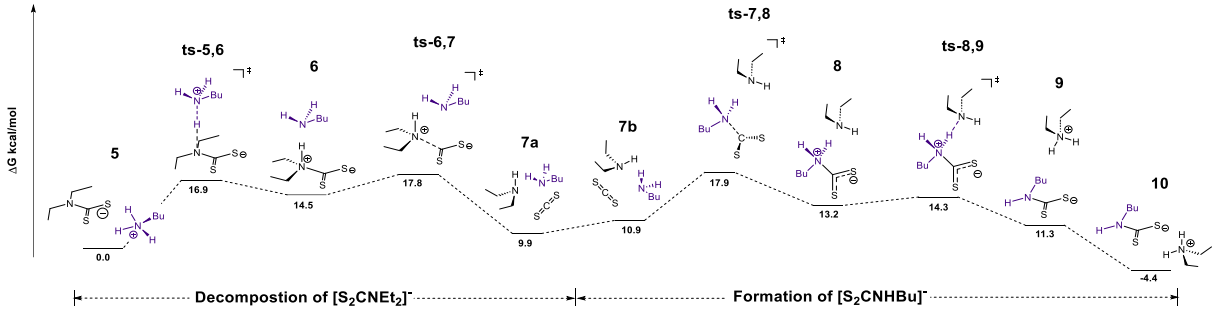

Figure S39. Full calculated reaction coordinate diagram for the transamidation of N,N-diethyldithiocarbamate with butylamine to give N-butyldithiocarbamate. In this reaction pathway, the fragments liberated in **7a** undergo a facile rearrangement to **7b** to allow the attack of the CS_2 by butylamine. The diethylamine previously liberated in **7a** ultimately acts as the base during the transformation from **8** to **9**. Intermediate **9** then rearranges barrierlessly to **10**.

XV. Supplemental References

1. S. Toso, D. Baranov, U. Filippi, C. Giannini and L. Manna, Collective Diffraction Effects in Perovskite Nanocrystal Superlattices, *Acc. Chem. Res.*, 2023, **56**, 66–76.
2. N. Doebelin and R. Kleeberg, Profex: A Graphical User Interface for the Rietveld Refinement Program BGMN, *J. Appl. Crystallogr.*, 2015, **48**, 1573–1580.
3. K. J. Cavell, J. O. Hill and R. J. Magee, Synthesis and Characterisation of Some Secondary Amine-Dithiocarbamate salts, *J. Inorg. Nucl. Chem.*, 1979, **41**, 1277–1280.
4. S. J. Visco and L. C. DeJonghe, Ionic Conductivity of Organosulfur Melts for Advanced Storage Electrodes, *J. Electrochem. Soc.*, 1988, **135**, 2905.
5. P. Kubelka and F. Munk, A Contribution to the Optics of Pigments., *Zeits F Tech Phys.*, 1931, **12**, 593.

6. P. Makuła, M. Pacia and W. Macyk, How to Correctly Determine the Band Gap Energy of Modified Semiconductor Photocatalysts Based on UV–Vis Spectra, *J. Phys. Chem. Lett.*, 2018, **9**, 6814–6817.
7. R. López and R. Gómez, Band-gap Energy Estimation from Diffuse Reflectance Measurements on Sol–Gel and Commercial TiO_2: A Comparative Study, *J. Sol-Gel Sci. Technol.*, 2012, **61**, 1–7.
8. H. Zhong, F. Pan, S. Yue, C. Qin, V. Hadjiev, F. Tian, X. Liu, F. Lin, Z. Wang and J. Bao, Idealizing Tauc Plot for Accurate Bandgap Determination of Semiconductor with Ultraviolet–Visible Spectroscopy: A Case Study for Cubic Boron Arsenide, *J. Phys. Chem. Lett.*, 2023, **14**, 6702–6708.
9. J. Tauc, R. Grigorovici and A. Vancu, Optical Properties and Electronic Structure of Amorphous Germanium, *Phys. Status Solidi B*, 1966, **15**, 627–637.
10. C. L. Raston and A. H. White, Crystal Structures of Tris(Diethyldithiocarbamato)-Antimony(III) and -Bismuth(III), *J. Chem. Soc. Dalton Trans.*, 1976, 791–794.